A case study on the seismic performance of earth dams

Loizos Pelecanos[1], Stavroula Kontoe[2], Lidija Zdravković[3]

[1] Research Associate, University of Cambridge. Formerly, Imperial College London, lp418@cam.ac.uk

[2]Senior Lecturer, Imperial College London, stavroula.kontoe@imperial.ac.uk

[3] Professor, Imperial College London, l.zdravković@imperial.ac.uk

Abstract

The seismic nonlinear behaviour of earth dams is investigated by using a well-documented case study and employing advanced static and dynamic coupled-consolidation finite element analysis. The static part of the analysis considers the layered construction, reservoir impoundment and consolidation, whereas the dynamic part considers the response of the dam to two earthquakes of different magnitude, duration and frequency content. The results of the analysis are compared with the recorded response of the dam and exhibit a generally good agreement. The effects of the narrow canyon geometry, the reservoir impoundment and the elasto-plastic soil behaviour on the seismic dam behaviour are investigated. Finally the implications of the adopted constitutive modelling assumptions on the predicted response are discussed.

1. Introduction

The early studies on the seismic response of dams followed the pseudo-static method of analysis (Terzaghi, 1950; Sarma, 1979) and aimed to calculate the minimum seismic load that could cause instability of the dam slope. Later, sliding block methods of analysis (Newmark, 1965; Ambraseys & Sarma, 1967; Ambraseys & Menu, 1988; Bray & Travasarou, 2007) concentrated on estimating the seismically induced permanent displacements.

More advanced shear beam analyses investigated the dynamic response of dams considering transverse (Ambraseys, 1960; Gazetas, 1982), vertical (Gazetas, 1981a) and longitudinal (Abdel-Ghaffar & Koh, 1981; Gazetas, 1981b) vibrations. Besides, the shear beam method was extended to consider the effects of canyon geometry (Dakoulas & Gazetas, 1987) and inhomogeneous dam materials (Abdel-Ghaffar & Koh, 1981; Gazetas, 1982; Dakoulas & Gazetas, 1985).

Subsequent finite element (FE) studies concentrated on the three-dimensional (3D) analysis of earth dams (Griffiths & Prevost, 1988; Dakoulas, 2012), elasto-plastic behaviour of the soil materials (Prevost et al., 1985; Woodward & Griffiths, 1996), hydrodynamic pressures on dams (Pelecanos et al., 2013), coupled-consolidation analysis (Lacy & Prevost, 1987; Sica et al., 2008, Elia et al., 2010) and estimation of critical seismic coefficients (Andrianopoulos et al., 2014, Papadimitriou et al., 2014) using constitutive models of various levels of complexity. The FE method is considered one of the most powerful tools to analyse the response of dams during earthquakes, however most of the numerical studies mentioned were not compared to field measurements and therefore their reliability is questioned.

This paper presents a numerical analysis of a dam case study, the La Villita earth dam in Mexico, with the objective of performing a "blind" prediction of the dam's behaviour using as input the available information about the foundation soils, materials of the dam structure and historic construction and earthquake records, to develop the numerical model. Both static and dynamic FE analyses are then performed to obtain the response of the dam during previous earthquakes and compare its predicted and recorded behaviour. The investigation considers the full stress-history of the dam, the coupled-consolidation behaviour of the materials and the effect of the 3D canyon geometry under two seismic events of distinct intensity. The aim of this study is to examine to what extent nonlinear FE analysis is able to reproduce the observed seismic dam response and to investigate the effects of some inevitable assumptions introduced in the numerical model.

2. La Villita dam

2.1. Description of the dam

La Villita is a 60m high zoned earth dam in Mexico with a slightly curved crest about 420m long, which is founded on an alluvium layer of varying thickness. The dam cross-section is composed of a central clay core of very low permeability, with sand filters and rockfill shells. Alluvial deposits beneath the clay core were grouted below the dam, while there is alsoa concrete cut-off wall to control seepage through the alluvium below the dam. Figures 1 and 2 show the transverse and longitudinal sections of the dam respectively.

The dam experienced six major seismic events during the period between 1975 and 1985 (Table 1). Although it did not fail, it sustained some deformations. The earthquake motions were recorded by three accelerometers which were installed on the dam soon after the end of construction. There is one instrument on rock at the right rock bank (point R in Figure 2) and two at the dam body which are located at the crest and the downstream berm (points C and B in Figures 1 and 2).

Table 1: Summary of earthquake events

No	Date	Ms	Epic. Dist. [km]	Max. Rock accel. [g]	Max. Berm accel. [g]	Max. Crest accel. [g]	Rock predom. period [sec]	Berm predom. period [sec]	Crest predom. Period [sec]
EQ1	11/10/1975	4.5	52	0.07	0.09	0.36	0.2	0.18	0.32
EQ2	15/11/1975	5.9	10	0.04	0.08	0.21	0.18	0.34	0.77
EQ3	14/3/1979	7.6	121	0.02	0.14	0.40	0.16	0.32	0.28
EQ4	25/10/1981	7.3	31	0.09	0.24	0.43	-	0.29	0.27
EQ5	19/11/1985	8.1	58	0.12	-	0.76	0.57	-	0.75
EQ6	21/11/1985	7.5	61	0.04	-	0.21	0.37	-	0.65

Not all three acceleration records in all three global directions are available. Some of the records are incomplete, containing only a small part of the actual record. Elgamal (1992) states that due to instrument malfunction at the right rock bank, only the bedrock records of 15 November 1975 (EQ2) and 19 November 1985 (EQ5) are useful for numerical analysis. Also, it should be noted that only a portion of the bedrock record of EQ2 is available (which can be used as input to a numerical analysis).

2.2. Previous research on La Villita dam

Because of the available ground motion data, a number of researchers have previously investigated this dam. Moreover, what attracted the researchers' attention was the asymmetry of the acceleration record of the crest of the dam, which showed higher values of acceleration in the positive (downstream) direction (Figure 12(a)). High values of peak acceleration could potentially suggest the existence of a localised failure with some permanent displacements, as the integration of an asymmetric acceleration record results in residual displacements (see Fig. 15). Elgamal et al. (1990) used a simple sliding block model to investigate the observed acceleration asymmetry concluding that the latter was the result of a localised slip failure, while Elgamal (1992) employed a 3D shear beam method to numerically analyse its performance during two earthquakes. Succarieh et al. (1993) used a 1D shear beam method to analyse the dynamic response of the dam and further utilised the Newmark (1965) sliding-block method to compute the permanent displacements.

Gazetas & Uddin (1994) developed a procedure for analysing earth dams in which, using pseudo-static slope stability analysis, a potential failure surface was identified. Finite element analysis (FE) was then performed with the pre-specified sliding surface behaving as perfectly plastic material (i.e. sliding occured when the acceleration exceeded the strength of the material), whereas the rest of the dam body behaved in a visco-elastic manner. The above-described method was applied on La Villita dam (Uddin, 1997) to investigate the observed response asymmetry. Two points on the two edges of the dam crest were monitored (one inside and one outside the sliding mass) and their response was compared, showing that the point inside the sliding mass presented an asymmetric acceleration response. Finally, Papalou & Bielak (2001, 2004) performed 3D numerical (combined FE and shear beam) elastic and elasto-plastic analyses of the dam with the surrounding canyon and showed that dam-canyon interaction results in smaller accelerations in the dam.

Based on the previous findings, the premise of the current study is that the observed acceleration record is the result of the combination of (a) the dynamic behaviour of the dam structure and (b) the high acceleration peaks due to a localised failure close to the monitoring instrument.

3. Numerical model

Finite element (FE) analyses, employing the Imperial College Finite Element Program (ICFEP) (Potts & Zdravković, 1999, 2001) are performed to analyse the response of the dam. Two-dimensional plane-strain static and dynamic in the time domain coupled-consolidation analyses are carried out in order to model the history of the dam prior to the earthquake events and its subsequent seismic response.

3.1. Stages of analysis

First, layered construction of the embankment is modelled over one year (1967), followed by one year of consolidation (1968). Then, water impoundment is simulated over six months (1969) followed by another long period of pure consolidation (6.5 years: 1969-1975), before the dynamic analysis of the first seismic event (EQ2 in 1975). Subsequently, a further period of 10 years of static consolidation is modelled before the final dynamic analysis of the second seismic event (EQ5 in 1985).

3.2. FE model geometry & boundary conditions

The FE mesh employed is shown in Figure 3. It consists of 1503 eight-noded isoparametric quadrilateral elements. Elements of consolidating materials (clay core and alluvium only) have also pore water pressure degrees-of-freedom at corner nodes. The maximum element size (6m) is chosen to be smaller than 1/5 of the smallest wavelength (lowest shear wave velocity over the highest frequency of the input wave). The highest considered frequency of the input motion is taken as 12Hz, which is determined from the Fourier Amplitude Spectra (FAS) of the two motions used. The cut-off value used is the frequency for which the corresponding Fourier Amplitude (FA) value becomes less than 10% of the highest value of FA (i.e. much higher than the predominant frequencies of the input records, predominant periods listed in Table 1).

The adopted deformation boundary conditions (BCs) for the static part of the analysis are: full fixity (displacements in both directions are zero) at the bottom boundary of the mesh and horizontal fixity (horizontal displacements are zero) at the lateral boundaries of the mesh. For the dynamic part of the analysis, the BCs along the bottom boundary are: fixity in the vertical direction and prescribed values of acceleration in the horizontal, whereas the tied-degrees-of-freedom (TDOF) BC was applied along the vertical sides of the alluvium layer in both directions. Hydrodynamic pressures are not taken into account in these simulations, because they are not considered significant for earth dams (Hall & Chopra, 1982; Gazetas, 1987; Pelecanos, 2013, Pelecanos et al, 2013). The reservoir hydrostatic pressures are used throughout the analysis. The bottom boundary of the mesh is placed at the interface between the foundation alluvium and the rigid bedrock, which is considered “infinitely” stiff, while the lateral boundaries are placed sufficiently far, so that interaction between them and the dam is avoided. The location of the latter boundaries was established after a parametric investigation, which compared the acceleration response at the far-field boundary of the model against the free-field response resulting from one-dimensional propagation from a column analysis of the alluvium layer. Figure 4 shows a comparison of the surface acceleration time history at point DB (see Figure 3) for the dynamic analysis during EQ2 (with the updated shear stiffness, see Section 5.1), and that computed at the top of a 70m deep column analysis representing the free-field response of the alluvium layer. The good agreement between the two time histories confirms the adequacy of the lateral size of the model and the associated boundary conditions.

3.3. Material properties & constitutive models

A summary of the properties of the materials of the dam are listed in Table 2. The properties are taken from Elgamal (1992), who does not mention what types of tests were carried out to characterise the material. All subsequent studies on this dam (Succarieh et al, 1993; Gazetas & Uddin, 1994; Papalou & Bielak, 2001, 2004) adopt the same properties listed in Elgamal (1992), without any additional information about them, or any new data. Following Elgamal (1992), a linear variation of the maximum shear stiffness, G_{max}, is used for all the materials in the dam embankment (140-260 MPa from top to bottom), whereas a constant value of 200 MPa is used in the alluvium. The values adopted for the permeability for the consolidating materials (clay and alluvium) are $K_{clay} = 1{\cdot}10^{-10}$ m/s and $K_{alluvium} = 1{\cdot}10^{-7}$ m/s. The remaining materials are considered to behave in a drained manner.

Table 2: Summary of known material properties

No	Material	Mass density	Poisson ratio	Cohesion	Angle of shearing	Angle of dilation
		ρ [kg/m^3]	ν [ ]	c' [kPa]	φ' [deg]	ψ [deg]
1	Clay core	2000	0.49	5	25	0
2	Sand filters	2180	0.33	0	35	0
3	Inner Rockfill	2080	0.33	5	45	0
4	Outer Rockfill	2080	0.33	5	45	0
5	Alluvium	2080	0.33	5	35	17.5

The constitutive model used is a cyclic nonlinear model (CNL), which adopts a logarithmic function to describe the backbone curve (Puzrin & Burland, 2000; Taborda, 2011) coupled with a Mohr-Coulomb failure criterion. The logarithmic relation (Equation A1) dictates the degradation of shear stiffness, G, and the increase of damping, ξ, with cyclic shear strain, γ. The relationships associated with the adopted CNL are presented in Appendix A.

Due to the lack of experimental data the CNL is calibrated on empirical relations. The Vucetic & Dobry (1991) curves are used for the clay core, the curves of Seed et al. (1986) are used for the sand filters and finally the curves of Rollins et al. (1998) are used for the rockfill and alluvium materials. Table 3 lists the results of the calibration. It should be noted that 200 MPa is the average value for the G_{max} within the dam. As the value of G_{max} affects the degradation of stiffness in the adopted constitutive model (see Appendix A), an average value was used in the calibration. The calibration for the CNL model (i.e. for the nonlinear elastic part) is shown graphically in Figure 5. It is recognised from the latter figure that the predicted value of damping decreases beyond a certain threshold deviatoric strain value ($E_{d,L}$), as the model assumes a linear deviatoric stress – deviatoric strain (J- E_d) relationship beyond this strain value $E_{d,L}$. Care is taken so that the calibration of the CNL model exhibits a good agreement with the adopted empirical curves within the strain range that is relevant in the examined problem. In this study, the strains do not exceed 0.1% (examples shown in Figures 19 (a) and (b)) and therefore the damping mismatch for γ>0.1% is not expected to have an impact on the predicted response.

Table 3: Calibration parameters for the Logarithmic CNL model (see also Appendix A)

Material	**Logarithmic CNL model parameters**				
	G_{max}	**E_{dL}**	**J_L**	**c**	**G_{min}**
	[MPa]	**[ ]**	**[kPa]**	**[ ]**	**[MPa]**
Clay core	200	0.0019	185	0.4	20
Sand filters	200	0.0014	65	1.0	20

Rockfill & Alluvium	200	0.0004	45	0.3	20

4. Static analysis

After establishing the initial stress conditions (i.e. level ground with K_o = 1-sinφ' and the water table at 2m depth), the embankment is constructed in 10 successive layers of 6m height over a period of 1 year. The clay core is considered to have suction due to its compacted nature and a value of tensile pore water pressure of 50 kPa is specified on construction of each clay core layer, whereas all the rest of the embankment materials were compacted on construction with zero pore pressure. Subsequently, one year of pure consolidation (no additional loading, only dissipation of excess pore pressures) is modelled and then water is impounded in the reservoir.

The reservoir impoundment is modelled over a total duration of 6 months and water level is raised over 10 time increments. Therefore, the water in the reservoir is modelled as an additional external hydrostatic boundary stress on the upstream face of the dam up to a height of 54m. Besides, an additional boundary stress is applied on the upstream riverbed alluvium equal to the maximum hydrostatic value. At the same time of the application of the external boundary stress, the pore pressure in the elements of the upstream rockfill and sand filters is prescribed to be in equilibrium with the externally applied boundary stress, i.e. hydrostatic.

The deformation BCs are previously described in Section 3.2. The hydraulic BCs are: along the bottom boundary zero flow is prescribed, whereas along the lateral boundaries no change in pore water pressure is prescribed, in order to maintain the initial hydrostatic conditions. The hydraulic BCs on the boundaries of the core are: no flow on the bottom and top boundaries, and precipitation BC on the two lateral sides of the core. The precipitation BC (Potts & Zdravković, 1999, 2001) is an advanced BC which allows the prescription of dual hydraulic conditions. It may act as a prescribed flow in one direction, or as a prescribed value of pore water pressure, u. On both US and DS core sides, it is specified that if the water pressure is more tensile in the core than on the core boundary, there is no flow of water into the core from the fill (which is dry and therefore u= 0). On the other hand, if the pore pressures in the core are more compressive (u>0) than those on the core boundary, then the pore water pressure value on the boundary is prescribed to be equal to zero. In that case, there is going to be flow of water from within the core, towards rockfill, with such a flow rate, that the value of the pore water pressure, u on the core boundary will be equal to zero. This is prescribed only during the construction phase, when the fill is dry. The reason for the use of this advanced BC is to avoid the unrealistic inflow of water in the core when there is suction during its construction. During and after reservoir impoundment, the hydraulic BCs for the upstream lateral boundary of the mesh are: the prescribed pore water pressures are increased according to the pore pressure change due to the water level rise. Moreover, the hydraulic BC on the upstream face of the core has prescribed values of the pore water pressure according to the elemental pore pressures prescribed within in the upstream rockfill (i.e. a hydrostatic variation). This allows water seepage through the core according to the value of the material permeability.

Figure 6 shows the pore water pressure distribution in the dam after water impoundment, whereas Figure 7 shows the flow net in the clay core. It is shown from the first figure that there are pore pressures in the upstream rockfill as a result of the water impoundment. This distribution is linear in the vertical direction as the water penetrates quickly in the coarse rockfill and hydrostatic conditions are established. Moreover, pore pressures drop in the clay core which means that the pressure reduces in the downstream side of the core, compared to the hydrostatic values on the upstream side. There is still some suction in the upper part of the clay core, which indicates that a part of the core is still not fully saturated. Besides, comparing the two parts of the foundation alluvium, the upstream part shows significantly higher values of water pressure which are a result of the reservoir water. As far as the flow net in the core is concerned, flow lines (black) and equipotential lines (grey) are clearly formed indicating seepage from the upstream to the downstream side of the clay core. Finally, Figure 8 shows the calculated and recorded settlement history of the dam crest prior to the EQ events which exhibit a good agreement. It is therefore confirmed that the static part of the analysis (construction and impounding) is satisfactorily captured and that the appropriate stress conditions within the dam prior to the seismic events are established.

5. Dynamic analysis

The seismic analysis of the response of the dam under the EQ2 and EQ5 seismic events is performed with dynamic-in-the-time-domain FE analysis. The time integration scheme employed is the generalised-αalgorithm of Chung & Hulbert (1993) which is able to use numerical damping and selectively filter the high frequency components (Kontoe, 2006; Kontoe et al. 2008). The deformation BCs are those described in Section 3.2 and the hydraulic BCs are the same as those adopted in the static analysis after the reservoir impoundment, discussed in Section 4. The right-bank (rock) acceleration records for EQ2 and EQ5 are used as input to the dynamic analyses (following Elgamal, 1992).

5.1. Effect of canyon geometry

Figure 9 shows the calculated and recorded accelerations and the associated response spectra for EQ5 respectively at the crest of the dam (Point C in Figure 3). It is observed that the calculated accelerations are found to be significantly smaller than the recorded ones. A similar trend is observed in the corresponding response spectra, where the calculated spectral acceleration, S_a, values are generally smaller than the recorded ones. Interestingly, the calculated values of the spectral acceleration S_a are found to be smaller than the recorded values for small values of the period, $T < 1.3$ s, and larger for large values of the period, $T > 1.3$ s. This implies that higher accelerations are observed for larger values of the fundamental period, which would occur if a softer (i.e. with a larger fundamental period) system was considered. Therefore, this shows that the calculated response of the dam is softer than the recorded.

It is long known (Hatanaka, 1952; Ambraseys, 1960; Mejia & Seed, 1983; Dakoulas & Gazetas, 1987) that dams built in narrow canyons exhibit a stiffer response than dams built in wide canyons. In this case, La Villita is a 60m high dam founded on a 70m alluvial deposit and its crest length is about 420m. Therefore, the canyon length over height, L/H ratio is equal to 420/(60+70) = 3.2. This implies that canyon effects could be significant and a 2D analysis would be inappropriate as the real problem is stiffer than the corresponding 2D plane strain model. Such a 2D analysis would be suitable for a wide canyon (L/H >4) (Ambraseys, 1960). In order to overcome this soft response of a 2D analysis, the stiffening effect of the canyon geometry is taken into account by increasing the material stiffness of the dam. A parametric study is carried out to determine the ratio of the new updated shear stiffness over the initial stiffness, which would provide the best match between the calculated and recorded response spectra. It is found that the shape of the response spectrum (and therefore the fundamental period of the dam) is improved if the shear modulus, $G_{max}(z)$, is increased by 3.5 times. Therefore, the updated value of the maximum shear stiffness, G^*_{max},for all the materials in the dam embankment is 490-910 MPa, and 700 MPa for the alluvium. Because the calibration of the CNL model depends on the value of G^*_{max}, a new calibration is carried out for these new updated values. The results of the new calibration are shown in Figure 10, whereas the corresponding parameters are shown in Table 4.

Table 4: New updated calibration parameters for the Logarithmic CNL model (see also Appendix A)

Material	**Logarithmic CNL model parameters**				
	G^*_{max}	**E^*_{dL}**	**J^*_L**	**c***	**G^*_{min}**
	[MPa]	**[ ]**	**[kPa]**	**[ ]**	**[MPa]**
Clay core	700	0.0005	220	0.4	70
Sand filters	700	0.0004	100	0.5	70
Rockfill & Alluvium	700	0.0009	280	0.4	70

Figures 11 (a) and 12 (a) show the calculated acceleration time histories at the crest of the dam for EQ2 and EQ5 respectively with the updated values of G^*_{max}. Likewise, Figures 11 (b) and 12 (b) show the corresponding response spectra for the two earthquakes respectively. The former figures show that the new calculated accelerations are found to be in much better agreement with the recorded values. It should be noted that the short-duration time-histories (e.g. EQ2) are due to the unavailability of the full records of some events.

Moreover, good agreement is also observed in the corresponding response spectra (Figures 11 (b) and 12 (b)) where the calculated spectral acceleration S_a values are closer to the corresponding recorded. The previously observed small and high values of amplification for smaller and larger values of the period respectively vanish and the calculated spectral accelerations exhibit large amplifications for the smaller values of the fundamental period. This shows that a better match of the fundamental period of the dam is achieved by increasing the material stiffness (shear modulus, G^*_{max}).

According to the study of Dakoulas & Gazetas (1987), the ratio of the fundamental period of vibration of a dam built in a narrow canyon, T_n, over that of a dam built in an infinitely wide canyon, T_w, for L/H = 3.2 and for various shapes of the canyon is: $T_n/T_w = 0.6 \sim 0.75$. In the present study, the updated value of the shear modulus is taken as $G^*_{max} = 3.5 \cdot G_{max}$. The shear wave velocity, V_s, is given by Equation 1 (where, ρ is mass density).

$$V_S^* = \sqrt{\frac{G}{\rho}} \qquad (1)$$

Therefore the updated value of the shear wave velocity, V^*_s is given by Equation 2.

$$V_S^* = \sqrt{3.5} V_S \qquad (2)$$

Finally, the fundamental period of vibration, T, is inversely proportional to the shear wave velocity (Ambraseys, 1960) and therefore, the new updated value of the fundamental period of vibration, T*, is given by Equation 3.

$$T^* = \frac{1}{\sqrt{3.5}} T = 0.54\, T \qquad (3)$$

Therefore, the ratio T*/T = 0.54 is close to the ratio suggested by Dakoulas & Gazetas (1987) (0.6 ~ 0.75) for various shapes of the canyon. This observation confirms that the calculated stiffening of the narrow canyon is in agreement with earlier work from the literature. However, the stiffening observed in the present study was found to be slightly larger, i.e. the ratio of T*/T is smaller than the ratio suggested in the literature. This difference could be attributed to the different assumptions of this work and the previous theoretical studies, i.e. an idealised geometry of earth dam and canyon geometries, and a linear soil material behaviour (see also Pelecanos (2013)). It could also be attributed to the uncertainty associated with the original material properties that are found from the literature (Elgamal, 1992). The increase of material stiffness was introduced to artificially take account of the 3D geometric stiffness due to a narrow canyon. Despite the good agreement of the response spectra and the amount of additional stiffening with analytical solutions, it should be recognised that the adoption of higher stiffness is not ideal, as this affects the predicted response in terms of shear strains and can also impact the prediction of topographic amplification effects which relate to the ratio of dam height to predominant wavelength of the response. An analysis considering the full 3D geometry of the dam-canyon problem should be able to provide a better insight into the complicated canyon-dam interaction and confirm the results of this study. However, recognising that an accurate full 3D nonlinear dynamic coupled-consolidation analysis is extremely computationally demanding, a 2D plane-strain analysis following the suggestions proposed in this study presents a reasonable compromise, as long as appropriate assumptions are made.

5.2. Dynamic response of the dam

Figure 13 shows the accelerations and associated response spectra at the berm of the dam for EQ2 (Point B in Figure 3). It is observed that, similar to the response at the crest, a very good agreement is achieved between the recorded and calculated response at the berm. It should be mentioned that no berm record is available for EQ5.

Moreover, the response spectrum of the dam crest response for EQ5 predicted by Elgamal (1992) is included in Figure 12 (b) for comparison. It is evident that the predicted response in this work is in better agreement with the recorded one than the response calculated by Elgamal (1992). The response spectrum of Elgamal (1992), obtained from a 3D shear beam analysis has a narrower frequency content and higher amplifications at the significant frequencies, whereas the broader frequency content of the spectrum from the present study matches better the low frequency spectral ordinates.

Those high acceleration values for high frequencies in the response spectrum of the recorded motion are believed to originate from asymmetric high peak values of acceleration observed in the recorded acceleration time-history at the crest of the dam for EQ5. These high peaks are believed to be due to a localised slope failure, as suggested by previous researchers (see Section 2.2), which was not predicted by the FE analysis in this study. The present numerical model does not include any pre-defined weak zones, as this aspect was already addressed in the work of Gazetas & Uddin (1994), and instead attempts a more direct "blind" prediction of the response. If the high frequencies are filtered from the recorded accelerations at the crest, a better agreement is obtained between the recorded and the calculated response. Figure 14 (a) shows a comparison between the filtered recorded accelerations at the crest for EQ5 and those calculated in this work, whereas Figure 14 (b) shows the associated response spectra. The filtering was performed using SeismoSignal (Antoniou & Pinho, 2004), adopting a 4^{th} order Bandpass Butterworth filter for frequencies higher than 4 Hz (i.e. periods smaller than 0.25s). The frequency for the filtering was obtained from a parametric study and was taken as the magnitude at which the high values of peak acceleration (due to the localised slip failure) vanish, rendering the record symmetric and consequently representative of the overall dynamic behaviour of the dam structure). The filtering does not filter out the predominant frequency of the input motion which is around 1.8Hz (i.e. period of 0.57s, shown graphically in Figure 14 (b)). The reason behind the filtering is that by eliminating the high values of peak accelerations (due to the localised slip) the remaining record shows the dynamic behaviour of the dam and this is used to check whether the vibration characteristics (e.g. fundamental period of vibration) have been predicted well by the adopted model. Besides, Figure 15 shows a comparison between the calculated and recorded (filtered and original) horizontal displacements at the crest of the dam for EQ5.

It is shown that the peak values of recorded accelerations vanish along with the observed asymmetry in the record leading to a better agreement between the calculated and recorded accelerations time-histories. Therefore, after filtering, the predicted response spectrum compares also very well with the one of the recorded motion. Finally, the recorded residual seismic displacements disappear and the calculated and recorded displacement time-histories agree very well.

Figure 16 shows the vectors of sub-accumulated displacement for the duration of EQ5, i.e. the deformations that occurred only due to and during the EQ5 seismic event (i.e. excluding the deformations from the previous static and EQ2 parts). It should be noted that the relative magnitudes of the vectors (rather than absolute) are important in this figure, as they show the mechanism of dam deformation. It is therefore shown that the deformations that occurred during the EQ5 seismic event are concentrated on the upstream part of the dam in the rockfill. No major failure is indicated, but some slope movements. However, the magnitude of these deformations is still very small and not comparable to the recorded vertical settlement of the crest during EQ5 (around 30cm). In the same figure, the value and orientation of maximum displacement (3.6cm) is represented by a grey vector and it is located at the upstream dam slope. Moreover, the maximum calculated vertical displacement at the crest is found to be around 1.5cm which is much smaller than the corresponding recorded value. This means that the calculated deformations resulting from the earthquake events are very small compared to the recorded values. Figure 17 shows the time-history of the calculated vertical displacements at the crest of the dam for EQ5.

Figure 18 shows the contours of stress level, S, in the dam during EQ5. The stress level, S is defined as the ratio of the current deviatoric stress, J_c, over the value of the deviatoric stress at yield conditions, J_y, at the same value of the mean effective stress, p' (see Equations 4 & 5, where σ'_1, σ'_2, σ'_3 are the principal stresses).

$$J = \frac{1}{\sqrt{6}}\sqrt{(\sigma_1' - \sigma_2')^2 + (\sigma_2' - \sigma_3')^2 + (\sigma_3' - \sigma_1')^2} \qquad (4)$$

$$p' = \frac{1}{3}(\sigma_1' + \sigma_2' + \sigma_3') \qquad (5)$$

Therefore, S, takes values from 0 to 1, and shows how close the stress state of the soil is to yielding. It is shown that the values of stress level generally go up to 0.8 (contour B) at some places within the upstream rockfill, the downstream alluvium and the downstream dam slope. However, the maximum value of S is close to 0.95 (contour C) and therefore the soil in the dam is generally found not to be at the yielding stress state after the end of the earthquake.

5.3. Dynamic soil behaviour

A better understanding of the seismic response of the dam can be obtained by observing the behaviour of the soil during the seismic events. Figure 19 shows (a) the shear stress-strain and (b) the strain time-history in the upstream rockfill (at the 1st Gauss integration point of element UR in Figure 3). It may be observed that the behaviour of the soil in the rockfill is slightly nonlinear exhibiting small hysteretic loops and an accumulation of some residual strain. However, the magnitude of the induced stress and strains (0.01%) seems to be very small to cause severe plastic yielding and induce major failure of the dam slope.

Figure 20 shows the stress paths, J-p', (see Equations 4 & 5) for elements in the upstream (UR) and downstream (DR) rockfill respectively (see Figure 3). The figure includes the stress paths for the whole analysis, i.e. the static and dynamic (both EQ2 and EQ5) parts. On the same figure, the Mohr-Coulomb yield surface (YS) is also plotted. It should be noted that the Mohr Coulomb YS is not constant, but changes with the Lode's angle, θ (see Potts &

Zdravković, 1999). In these figures, the YS plotted corresponds to the point that the YS was first engaged, i.e. the first time that plastic strain developed at that point. However, it should be commented that the YS was found not to change considerably during the analysis. It is shown that for the upstream rockfill, the stress path approaches the yield surface and travels along it at around J = 100 kPa and p'= 120 kPa. This means that at that instant plasticity is introduced, which leads to permanent values of shear strain, as shown in Figure 19 (b).

Plasticity is not introduced in the downstream rockfill, as the stress paths are far away from the yield surface. It is shown that the reservoir impoundment causes a change in the direction of the stress path, as it results in smaller values of the mean effective stress, p', and brings the stress path closer to the yield surface. This is why more plasticity is introduced in the upstream rockfill.

5.4. Comments

The high peak values of acceleration observed in the recorded acceleration and already attributed by previous researchers to a localised failure close to the monitoring instrument were not captured. Such a localised failure was not predicted, from the inspection of the vectors of displacement plot after the earthquake. Nevertheless, when the high frequencies (originating from the localised slip failure) from the recorded accelerations are filtered, an excellent agreement is obtained between the calculated and recorded accelerations and response spectra. This shows that the dynamic response of the dam is well captured and the frequency content of the resulting calculated crest accelerations match the recorded.

It is believed that the failure of this study to predict the high values of recorded acceleration and the recorded displacements could be due to the possible pre-existence of a discontinuity in the embankment. Following the conclusions of previous researchers (Elgamal et al., 1990; Elgamal, 1992; Succarieh et al., 1993; Gazetas & Uddin, 1994; Uddin, 1997), it is suggested that perhaps some minor localised failure at the position close to the monitoring instrument may have happened before, which could have created a local discontinuity. This could have originated possibly from a previous seismic event or even from some construction processes. If such a discontinuity exists, it can form a weak zone in the dam and will be sensitive to seismic loads. As far as modelling is concerned, the adopted procedure in this work assumes uniform materials in the dam body, without artificial inclusion of weak zones, such as those in the work of Gazetas & Uddin (1994).

The observed asymmetry in the crest accelerations for EQ5 was also observed in previous strong events, e.g. EQ3 and EQ4 (Elgamal, 1992; Pelecanos, 2013), and therefore it is not unreasonable to assume that these events introduced gradually a shear surface in the vicinity of the crest. However, the unavailability of reliable and useful input motions for all the prior seismic events is a significant obstacle in performing a series of successive seismic analyses of all the previous earthquakes and hence appropriately model the development of plastic strains in the dam which might have created a sliding surface that can cause asymmetric crest accelerations. This highlights the importance of modelling all the previous events (including prior earthquakes) before the studied earthquake so that appropriate stress states are modelled.

Finally, if reliable input motions for all the seismic events were available, along with adequate experimental data from advanced tests performed on materials of the dams, then an advanced constitutive model, such as kinematic hardening model of the type employed in Kontoe et al. (2011), could be adopted to introduce early plasticity in the dam and potential strain softening in dam materials, in order to predict more reliably the occurrence of localised failure.

6. Conclusions

This paper describes the numerical study carried out to investigate the static and dynamic behaviour of La Villita dam. The dam is considered to be a reasonably well-documented case study because of the available information, i.e. material properties and monitored response. The dam is analysed in both static and dynamic conditions, considering nonlinear elasto-plastic soil behaviour. Two-dimensional plane-strain coupled-consolidation static and dynamic FE analyses are performed.

The aim of this investigation is to "blindly" analyse (using existing constitutive models) the observed seismic response of an earth dam, for which certain (material and earthquake) data are available. In summary, it is believed that this study:

- has been successful in (a) predicting the overall dynamic behaviour of the dam structure for two earthquakes of different magnitude, duration and frequency content; and (b) demonstrating (indirectly by careful filtering of the record) the validity of the assumption taken from the studies by previous researchers that the observed acceleration asymmetry and large displacements have likely resulted from localised failure near the measuring instrument;
- showed that increasing the stiffness of the dam materials in a 2D analysis, using a carefully designed parametric study, is an acceptable approximate way to take account of the stiffening effect of the 3D canyon (good prediction of the fundamental period of vibration, shown by the response spectra). The amount of stiffening agrees reasonably well with previous linear analytical solutions (Dakoulas & Gazetas, 1987) and therefore the developed numerical model may be considered as verification of these analytical solutions.
- examined whether a uniform continuum model (i.e. without introducing a pre-determined localised weak zone, either by interface elements or by decreasing locally the stiffness) can fully reproduce the observed localised deformations and corresponding asymmetric accelerations. In this case, it is anticipated that the dam materials may not be uniform in the field (i.e. there could be a localised discontinuity). As a consequence, any uniform continuum model would find it difficult to fully capture the observed behaviour.

Acknowledgements

The first author would like to express his acknowledgements to the Engineering and Physical Sciences Research Council (EPSRC), UK for the award of a Research Studentship for his PhD studies at Imperial College.

Appendix A

The cyclic nonlinear model (CNL) adopted in this work has 4 distinct parameters: the initial (maximum) shear stiffness G_{max}, the limit strain $E_{d,L}$, the limit stress $J_{d,L}$ and c which is the inclination coefficient of the linear part of the stress-strain curve (the stress strain curve is linear beyond the point $J_{d,L}$, $E_{d,L}$). The parameters $E_{d,L}$, $J_{d,L}$ control mainly the shape of the stiffness and damping curves for small to medium strain levels, while the parameter c controls the residual secant stiffness and the maximum damping ratio.

The backbone curve is described by the logarithmic relation in Equation A1.

$$\boldsymbol{J = E_d G_{max}\left\{1 - \alpha\left[\ln\left(1 + \frac{|E_d| G_{max}}{J_L}\right)\right]^R\right\}} \qquad \text{(A1)}$$

where J and E_d are the stress and strain invariants respectively, whereas α and R are auxiliary constants defined by Equations A2 and A3.

$$\boldsymbol{\alpha = \frac{x_L - 1}{\chi_L[\ln(1+\chi_L)]^R}} \qquad \text{(A2)}$$

$$\boldsymbol{R = \frac{c(1+\chi_L)ln(1+\chi_L)}{\chi_L(\chi_L - 1)}} \qquad \text{(A3)}$$

And χ_L is defined by Equation A4.

$$\boldsymbol{\chi_L = \frac{E_{dL}}{J_L} G_{max}} \qquad \text{(A4)}$$

Then, the stress-strain behaviour is defined by Equation A5.

$$\boldsymbol{J = J_r + (E_d - E_{dr})G_{max}[1 - \alpha L^R]} \qquad \text{(A5)}$$

where J_r, E_{dr} are the deviatoric stress and strain respectively at the last known reversal point, whereas L is defined by Equation A6.

$$\boldsymbol{L} = \boldsymbol{ln}\left(\boldsymbol{1} + \frac{\boldsymbol{G_{max}}|\boldsymbol{E_d} - \boldsymbol{E_{dr}}|}{\boldsymbol{nJ_L}}\right) \qquad \text{(A6)}$$

where n is a Masing rule scaling factor of the backbone curve, which becomes 1 for initial loading and 2 during and after the first stress reversal.

The CNL model follows a non-linear (logarithmic) relation for J and E_d for very small strains up to $J=J_L$, $E_d=E_{dL}$ and then it follows a linear relationship with stiffness (slope) G_{imp} defined by Equation A7.

$$\boldsymbol{G_{imp}} = \boldsymbol{G_{max}} \frac{(\boldsymbol{1} - \boldsymbol{c})}{\boldsymbol{X_L}} \qquad \text{(A7)}$$

There is also an option in the model to specify a minimum value of shear stiffness, G_{min} which functions as long as the value of G_{min} is larger than G_{imp}. A constant value of Poisson's ratio is used to calculate the bulk modulus.

In the present study the CNL model is used in conjunction with a Mohr-Coulomb (MC) failure envelope. A sub-stepping stress-point algorithm is employed at all times for accurate integration of constitutive equations (as explained in Potts & Zdravkovic, 1999). In such coupling the linear elasticity of the standard MC model which requires two input parameters, a Young's modulus and a Poisson's ratio, or a shear, G, and a bulk, K, moduli, is replaced by the nonlinear elastic CNL model. CNL defines a nonlinear elastic shear modulus and, with the addition of a constant Poisson's ratio, also the nonlinear elastic bulk modulus. While the stress state is below the MC envelope, the material behaviour is governed by the CNL model. Once the MC envelope is reached, plastic strains accumulate and the backbone curve is controlled by the MC model. When a reversal occurs and the stress path moves away from the MC envelope within the elastic area, the hardening parameters are accordingly updated.

Nomenclature

a acceleration

c cohesion

E_d deviatoric strain

G shear modulus

H height of the dam

J deviatoric stress

J_L calibration parameter of the Logarithmic CNL model

K permeability

L length of the dam crest

p’ mean effective stress

R calibration parameter of the Logarithmic CNL model

S stress level

S_a spectral acceleration

t time

T period of vibration

u pore water pressure

v Poisson ratio

V_s shear wave velocity

α calibration parameter of the Logarithmic CNL model

γ shear strain

ε normal strain

ρ mass density

σ normal stress

τ shear stress

φ angle of shearing resistance

χ_L calibration parameter of the Logarithmic CNL model

ψ angle of dilation

References

Abdel-Ghaffar, A. M. & Koh, A. S. (1981) Longitudinal vibration of non-homogeneous earth dams. Earthquake Engineering and Structural Dynamics, 9, No. 3, 279-305.

Ambraseys, N. N. (1960) On the shear response of a two-dimensional truncated wedge subjected to arbitrary disturbance. Bulletin of the Seismological Society of America, 50, No. 1, 45-56.

Ambraseys, N. N. & Menu, J. M. (1988) Earthquake-induced ground displacement. Earthquake Engineering and Structural Dynamics, 16, No. 7, 985-1006.

Ambraseys, N. N. & Sarma, S. K. (1967) The response of earth dams to strong earthquakes. Géotechnique, 17, No. 2, 181-213.

Andrianopoulos, K., Papadimitriou, A. G., Bouckovalas, G. D. & Karamitros, D. K. (2014) Insight into the seismic response of earth dams with an emphasis on seismic coefficient estimation. Computers and Geotechnics, 55, 195-210.

Antoniou, S. & Pinho, R. (2004) SeismoSignal: A computer program for signal processing of strong-motion data. Technical Report 4.0.0, SeismoSoft.

Bray, J. D. & Travasarou, T. (2007) Simplified procedure for estimating earthquake-induced deviatoric slope displacements. Journal of Geotechnical and Geoenvironmental Engineering, ASCE. 133, No. 4, 381-392.

Hall, J. F. & Chopra, A. K. (1982) Hydrodynamic effects in earthquake response of embankment dams. Journal of the Geotechnical Engineering Division, ASCE, 108, No.4, 591-597.

Chung, J. & Hulbert, G. M. (1993) A time integration algorithm for structural dynamics with improved numerical dissipation: the generalised-α method. Journal of Applied Mechanics, 60, 371-375.

Dakoulas, P. & Gazetas, G. (1985) A class of inhomogeneous shear models for seismic response of dams and embankments. Soil Dynamics and Earthquake Engineering, 4, No. 4, 166-182.

Dakoulas, P. & Gazetas, G. (1987) Seismic lateral vibration of embankment dams in semi-cylindrical valleys. Earthquake Engineering and Structural Dynamics, 13, No. 1, 19-40.

Elgamal. A. W., Scott, R. F., Succarieh, M. F. & Yan, L. (1990) La Villita dam response during five earthquakes including permanent deformation. Journal of Geotechnical Engineering, 116, No. 10, 1443-1462.

Elgamal, A. W. (1992) Three-dimensional seismic analysis of La Villita dam. Jounal of Geotechnical Engineering, 118(12), 1937-1958.

Elia, G., Amorosi, A., Chan, A. & Kavvadas, M. J. (2010) Fully coupled dynamic analysis of an earth dam. Géotechnique, 61, No. 7, 549-563.

Gazetas, G. (1981a) Vertical oscillation of earth and rockfill dams: Analysis and field observation. Soils & Foundations, 21, No. 4, 56-68.

Gazetas, G. (1981b) Longitudinal vibrations of embankment dams. Journal of Geotechnical Engineering, ASCE, 107, No. 1, 21-40.

Gazetas, G. (1982) Shear vibrations of vertically inhomogeneous dams. International Journal for Numerical and Analytical Methods in Geomechanics, 6, No. 1, 219-241.

Gazetas, G. (1987) Seismic response of earth dams: some recent developments, Soil Dynamics and Earthquake Engineering, 6, No.1, 3-47.

Gazetas, G. & Uddin, N. (1994) Permanent deformation on pre-existing sliding surfaces in dams. Journal of Geotechnical Engineering, 120, No. 11, 2041-2061.

Griffiths, D. V. & Prevost, J. H. (1988) Two- and three-dimensional dynamic finite element analyses of the Long Valley dam. Géotechnique, 38, No. 3, 367-388.

Hatanaka, M. (1952) Three-dimensional consideration on the vibration of earth dams. Journal of the Japanese Society of Civil Engineers, 37, No. 10, 305-332.

Kontoe, S. (2006) Development of time-integration schemes and advanced boundary conditions for dynamic geotechnical analysis. PhD thesis, Imperial College London.

Kontoe, S., Zdravković, L. & Potts, D. M. (2008) Assessment of time-integration schemes for dynamic geotechnical problems. Computers and Geotechnics, 35, No. 2, 253-364.

Kontoe, S., Zdravković, L. & Potts, D. M. (2011) On the relative merits of simple and advanced constitutive models in dynamic analysis of tunnels. Géotechnique, 61, No. 10, 815-829.

Lacy, S. & Prevost, J. H. (1987) Nonlinear seismic response analysis of earth dams. Soil Dynamics and Earthquake Engineering, 6, No. 1, 48-63.

Mejia, L. H. & Seed, H. B. (1983) Comparison of 2D and 3D dynamic analyses of earth dams. Journal of Geotechnical Engineering, ASCE, 109, No. 11, 1383-1398.

Newmark, N. M. (1965) Effects of earthquakes on dams and embankments. Géotechnique, 15, No. 2, 139-160.

Papadimitriou, A. G., Bouckovalas, G. D. & Andrianopoulos, K. I. (2014) Methodology for estimating seismic coefficients for performance-based design of earth dams and tall embankments. Soil Dynamics and Earthquake Engineering, 56, 57-73.

Papalou, A. & Bielak, J. (2001) Seismic elastic response of earth dams with canyon interaction. Journal of Geotechnical and Geoenvironmental Engineering, 127, No. 5, 446-453.

Papalou, A. & Bielak, J. (2004) Nonlinear seismic response of earth dams with canyon interaction. Journal of Geotechnical and Geoenvironmental Engineering, 130, No. 1, 103-110.

Pelecanos, L., Kontoe, S. & Zdravković, L. (2013) Numerical modelling of hydrodynamic pressures on dams. Computers and Geotechnics, 53, 68-82.

Pelecanos, L. (2013) Seismic response and analysis of earth dams. PhD thesis. Imperial College London.

Potts, D. M. & Zdravković, L. (1999) Finite element analysis in geotechnical engineering: Theory. London: Thomas Telford.

Potts, D. M. & Zdravković, L. (2001) Finite element analysis in geotechnical engineering: Application. London: Thomas Telford.

Prevost, J. H., Abdel-Ghaffar, A. M. & Lacy, S. J. (1985) Nonlinear dynamic analyses of an earth dam. Journal of Geotechnical Engineering, 111, No. 7, 882-897.

Puzrin, A. M. & Burland, J. B. (2000) Kinematic hardening plasticity formulation of small strain behaviour of soils. International Journal of Numerical and Analytical Methods in Geomechanics, 24, No. 9, 753-781.

Rollins, K., Evans, M., Diehl, N,, & Daily, W. (1998) Shear modulus and damping relations for gravel. Journal for Geotechnical and Geoenvironmental Engineering, ASCE, 124, No. 5, 396-405.

Sarma, S. K. (1979) Stability analysis of embankments and slopes. Journal of Geotechnical Engineering, ASCE, 105, No. GT5, 1511-1524.

Seed, H. B., Wong, R. T., Idriss, I. M. & Tokimatsu, K. (1986) Moduli and damping factors for dynamic analyses of cohesionless soils. Journal of Geotechnical Engineering, 112, No. 11, 1016-1032.

Sica, S., Pagano, L. & Modaressi, A. (2008) Influence of past loading history on the seismic response of earth dams. Computers and Geotechnics, 35, No. 1, 61-85.

Succarieh, M. F., Elgamal, A. W. & Yan, L. (1993) Observed and predicted earthquake response of La Villita dam. Engineering Geology, 34, No. 93, 11-26.

Taborda, D. M. G. (2011) Development of constitutive models for application in soil dynamics. PhD thesis, Imperial College London.

Taborda D.M.G. , Zdravkovic L., Kontoe S., Potts D.M. (2010), Alternative formulations for cyclic nonlinear elastic models: Parametric study and comparative analyses, in Proc. of Numerical Methods in Geotechnical Engineering (NUMGE), Benz & Nordal (eds), Trondheim, Norway, 423-428.

Terzaghi, K. (1950) Mechanics of landslides. Technical Report Engineering Volume, The Geological Survey of America.

Uddin, N. (1997) A single-step procedure for estimating seismically-induced displacements in earth structures. Computers and Structures, 64, No. 5/6, 1175-1182.

Vucetic, M. & Dobry, R. (1991) Effect of soil plasticity of cyclic response. Journal of Geotechnical Engineering, 117, No. 1, 87-107.

Woodword, P. K. & Griffiths, D. V. (1996) Influence of viscous damping in the dynamic analysis of an earth dam using simple constitutive models. Computers and Geotechnics, 19, No.3, 245-263.

List of Figure captions

Figure 1: Cross-sectional view of La Villita dam.

Figure 2: Longitudinal section of La Villita dam and canyon.

Figure 3: FE mesh used in the analysis of La Villita dam.

Figure 4: Comparison of free-field accelerations for EQ2 from the downstream boundary edge of the FE mesh and from the top of a 70m alluvium column analysis.

Figure 5: Calibration of the CNL model against empirical curves: (a) stiffness degradation and (b) damping.

Figure 6: Contours of pore water pressure in the dam after the end of the reservoir impoundment.

Figure 7: Flow net (contours of stream and potential functions) in the clay core after the end of the reservoir impoundment.

Figure 8: Calculated and recorded crest settlement history of the dam crest prior to the EQ events.

Figure 9: Comparison of calculated results and recorded data at the crest of the dam for EQ5: (a) acceleration time-history and (b) response spectra.

Figure 10: New updated calibration of the CNL model against empirical curves: (a) stiffness degradation and (b) damping.

Figure 11: Comparison of calculated results and recorded data at the crest of the dam for EQ2 with the new updated material parameters: (a) acceleration time-history and (b) response spectra.

Figure 12: Comparison of calculated results and recorded data at the crest of the dam for EQ5 with the new updated material parameters: (a) acceleration time-history and (b) response spectra.

Figure 13: Comparison of calculated results and recorded data at the berm of the dam for EQ2 with the new updated material parameters: (a) acceleration time-history and (b) response spectra.

Figure 14: Comparison of calculated results and filtered recorded data at the crest of the dam for EQ5 with the new updated material parameters: (a) acceleration time-history and (b) response spectra.

Figure 15: Comparison of calculated and recorded horizontal displacements at the crest of the dam for EQ5 with the new updated material parameters.

Figure16: Vectors of sub-accumulated displacements at the end of EQ5.

Figure 17: Calculated vertical displacement time-history at the crest of the dam for EQ5.

Figure 18: Contours of stress level at the end of EQ5.

Figure 19: Calculated dynamic soil behaviour in the upstream rockfill (element UR) during EQ5: (a) shear stress-strain and (b) shear strain time-history.

Figure 20: Stress paths for the whole duration of the numerical static and dynamic analysis: (a) upstream rockfill (element UR) and (b) downstream rockfill (element DR).

Figure
Click here to download Figure: PelecanosFig01.eps

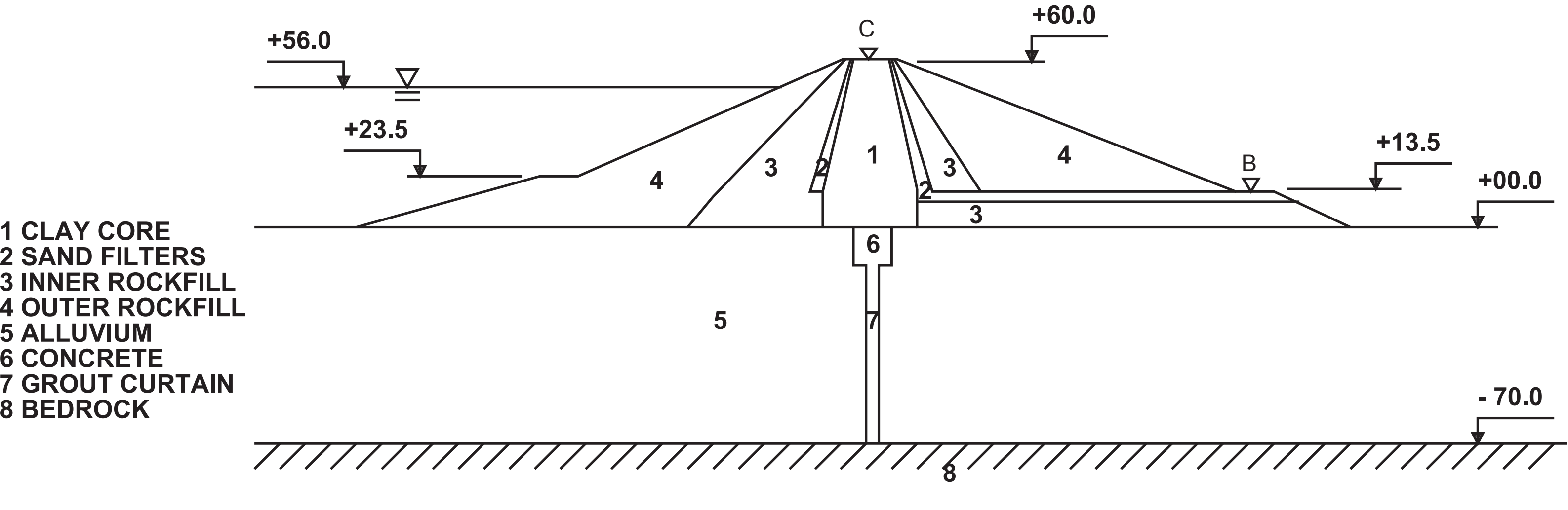

Figure
Click here to download Figure: PelecanosFig02.eps

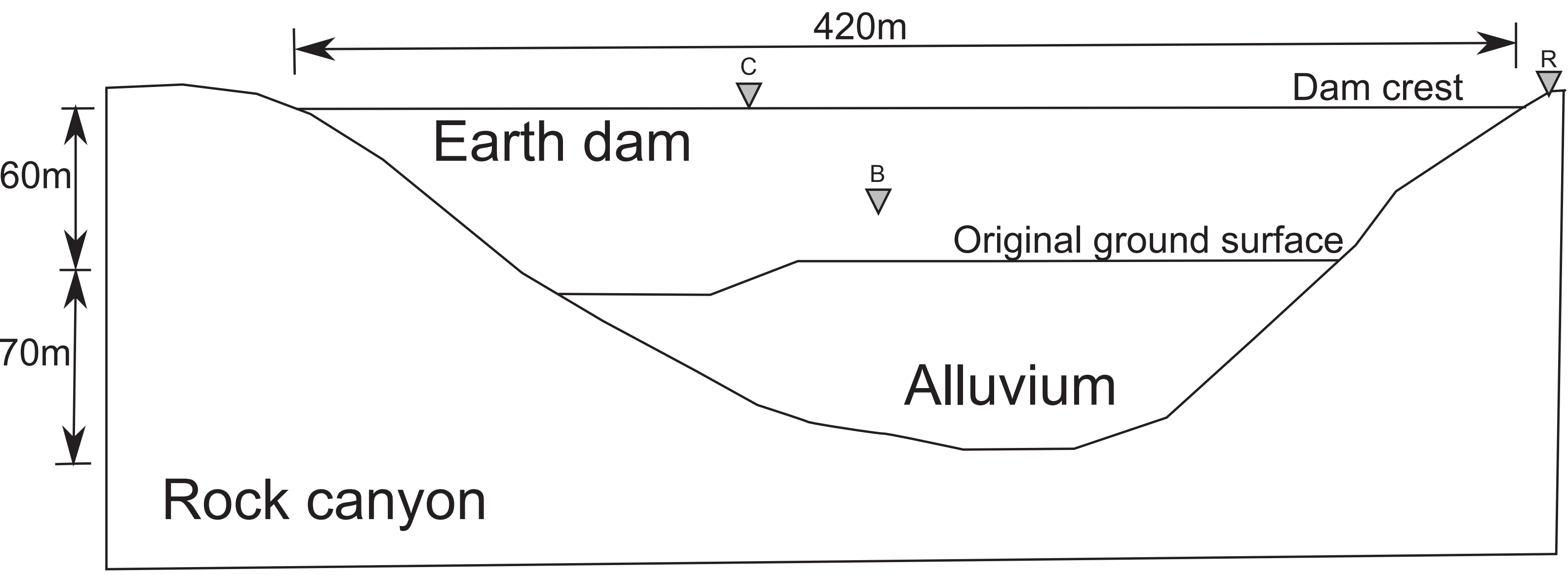

Figure
Click here to download Figure: PelecanosFig03.eps

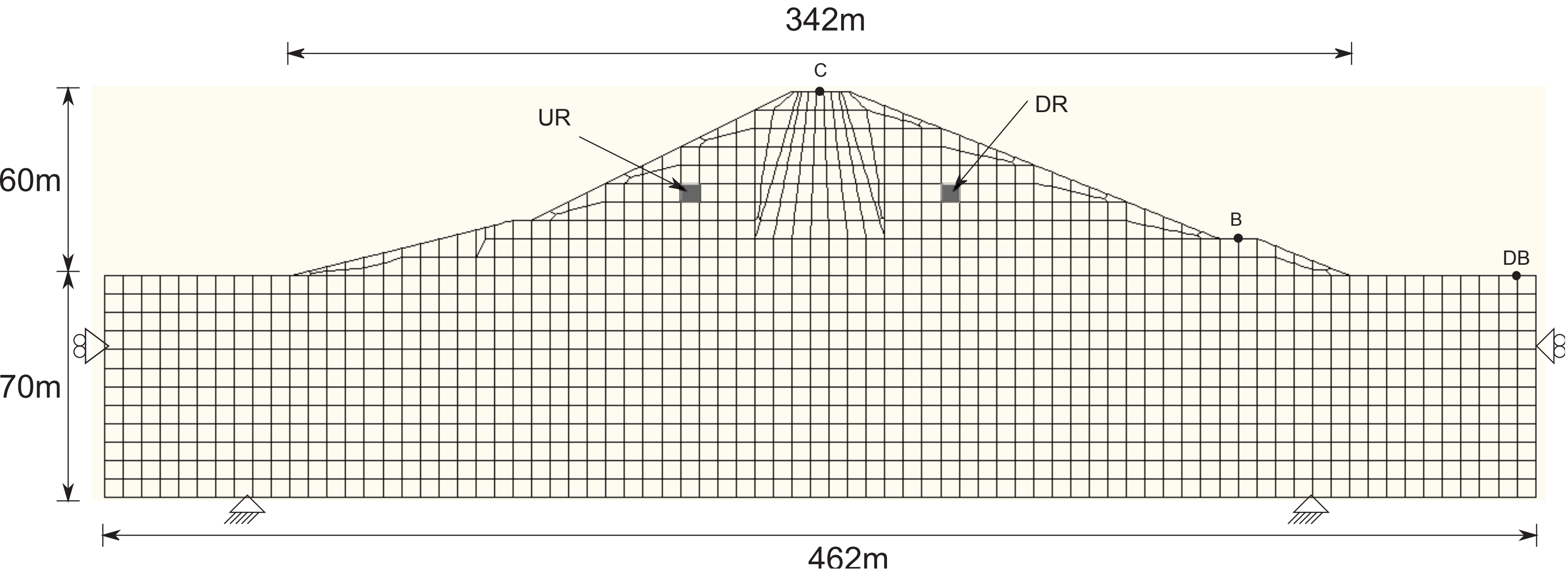

Figure
Click here to download Figure: PelecanosFig04.eps

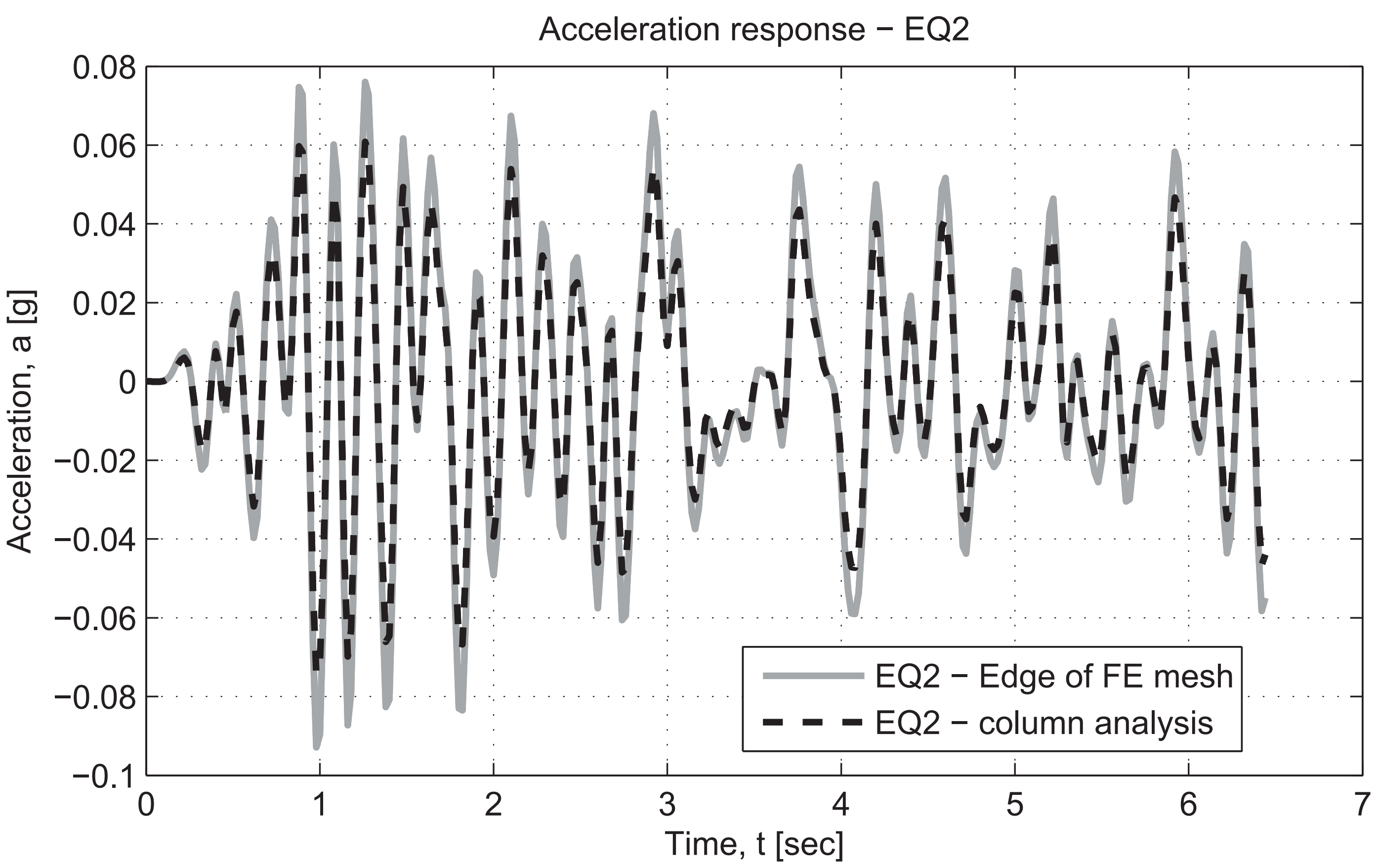

Figure
Click here to download Figure: PelecanosFig05a.eps

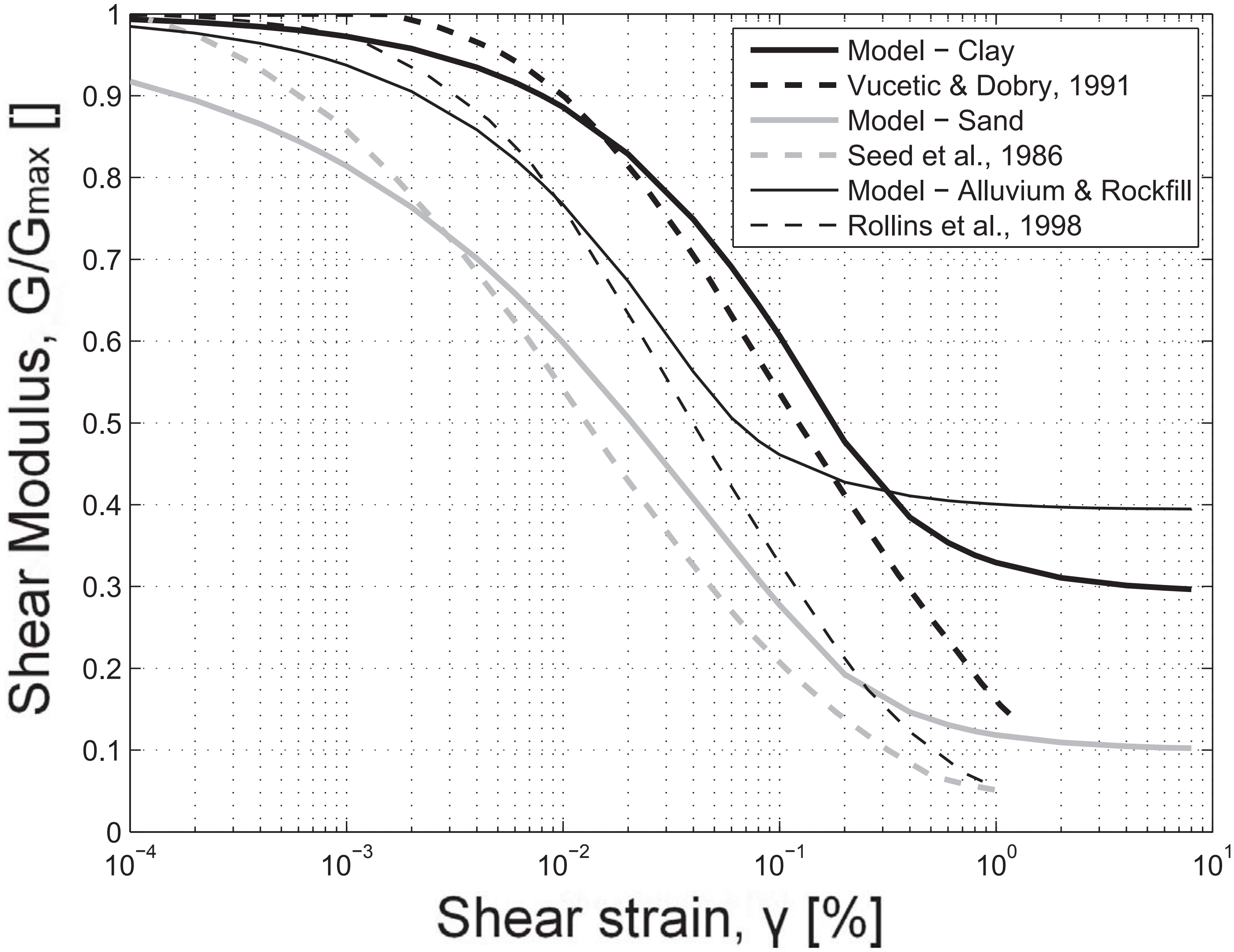

Figure
Click here to download Figure: PelecanosFig05b.eps

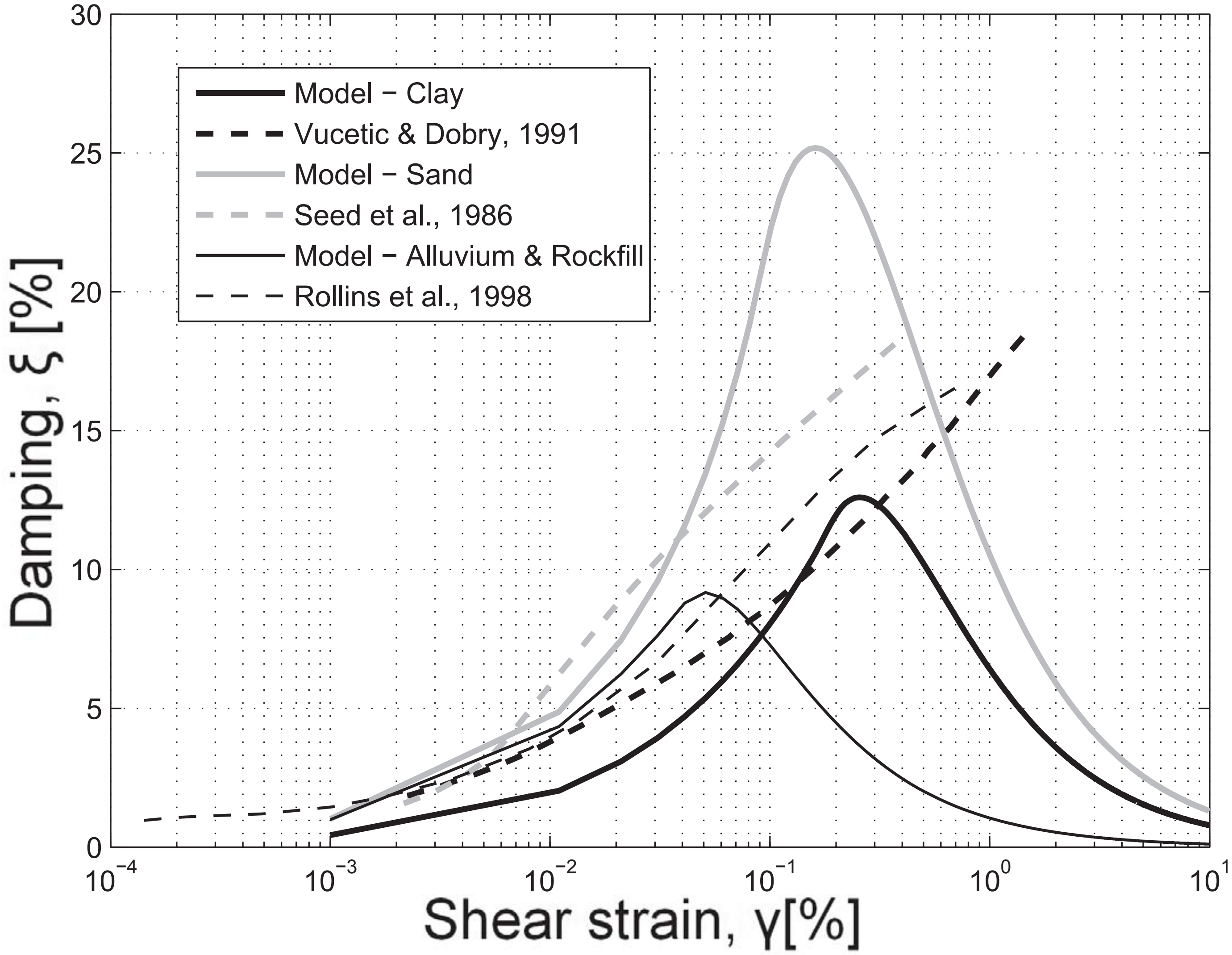

Figure
Click here to download Figure: PelecanosFig06.eps

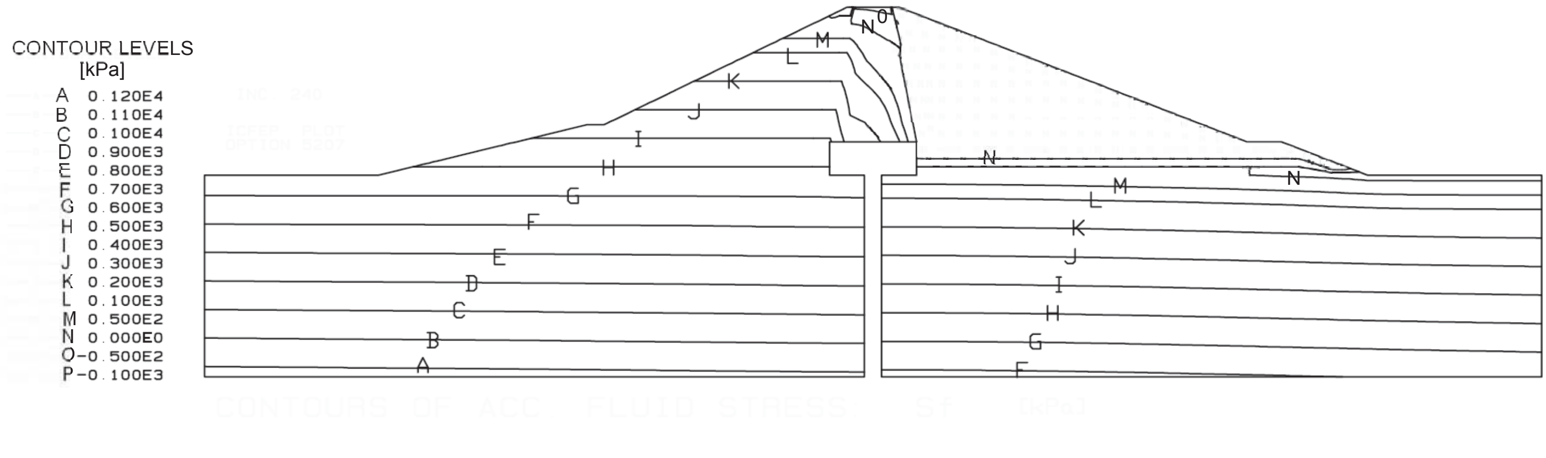

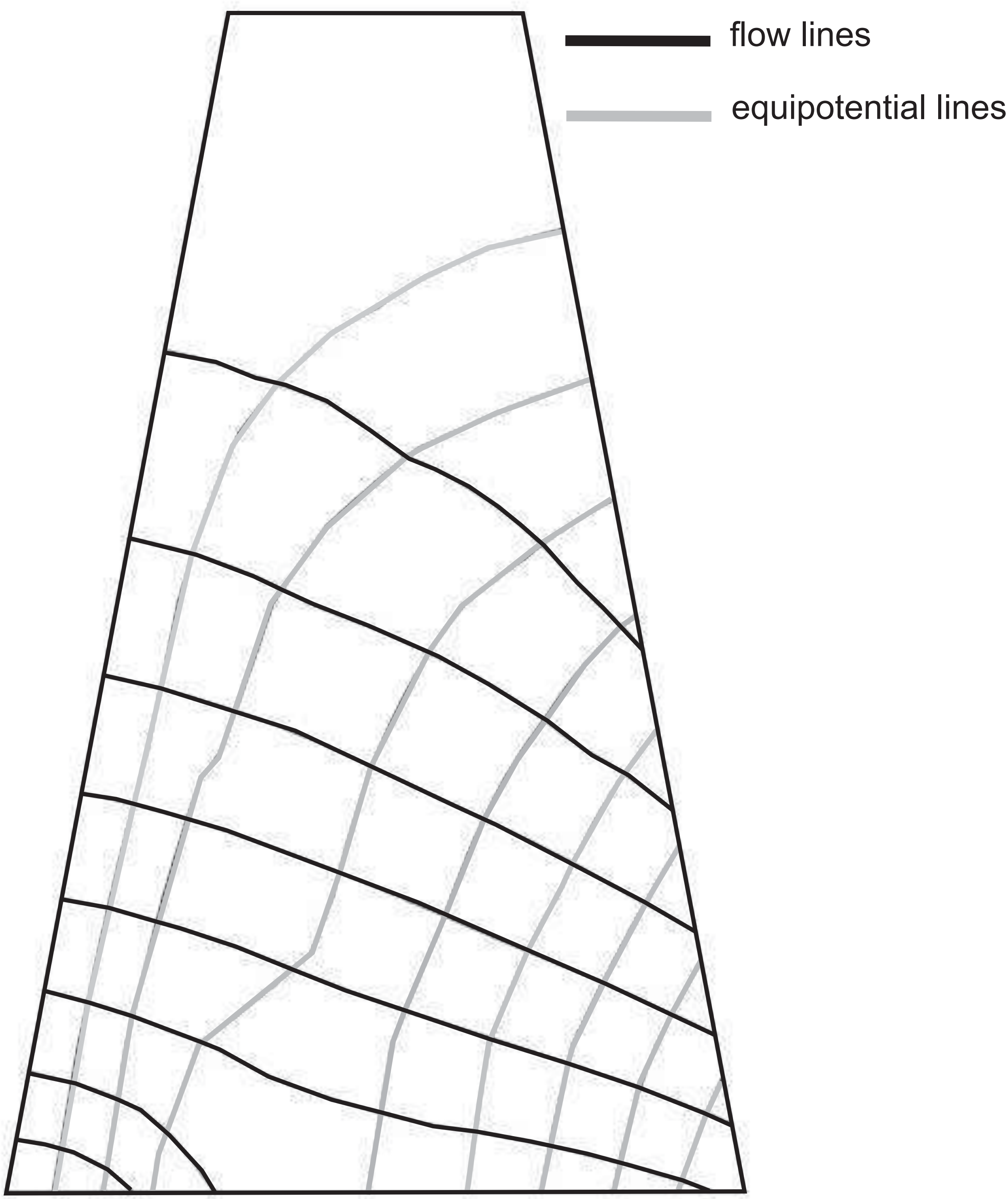
flow lines
equipotential lines

Figure
Click here to download Figure: PelecanosFig08.eps

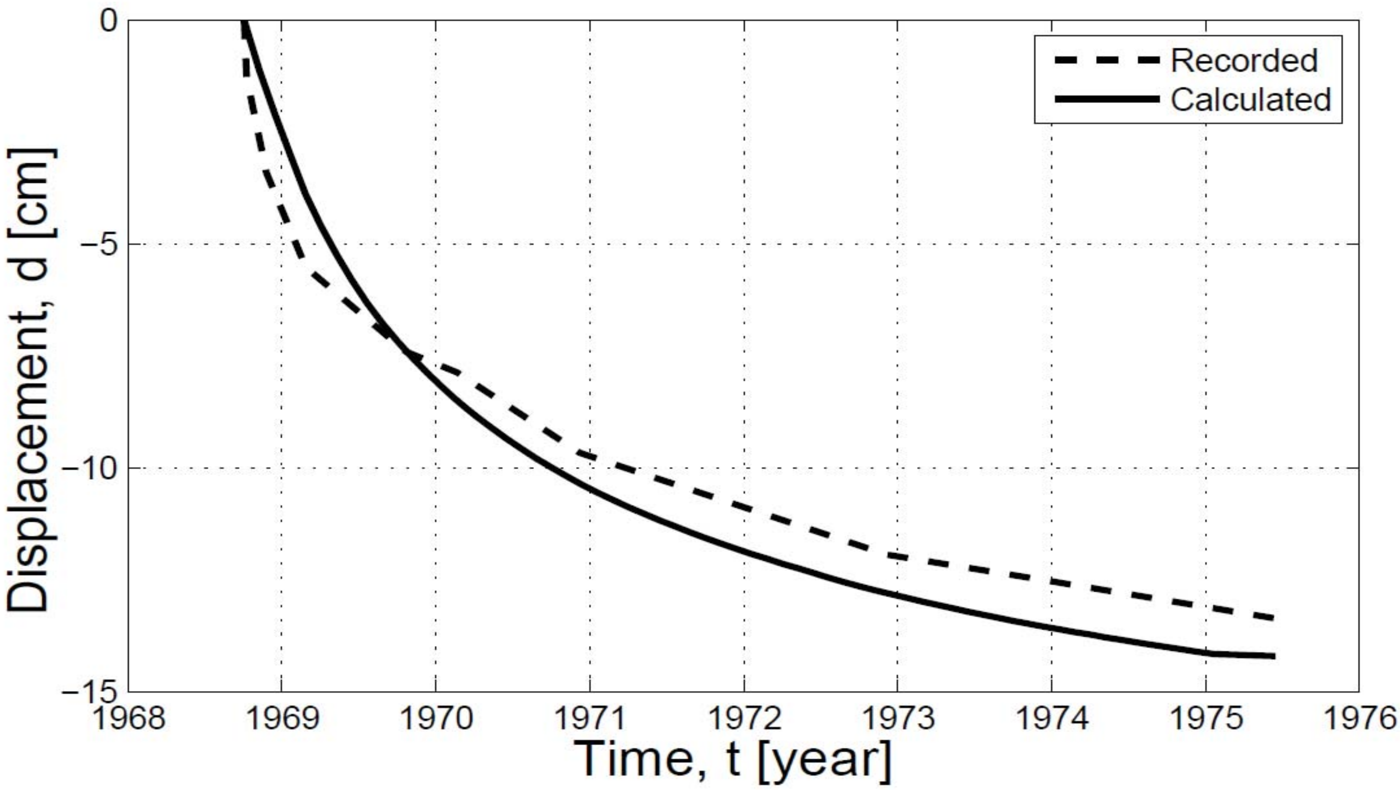

Figure
Click here to download Figure: PelecanosFig09a.eps

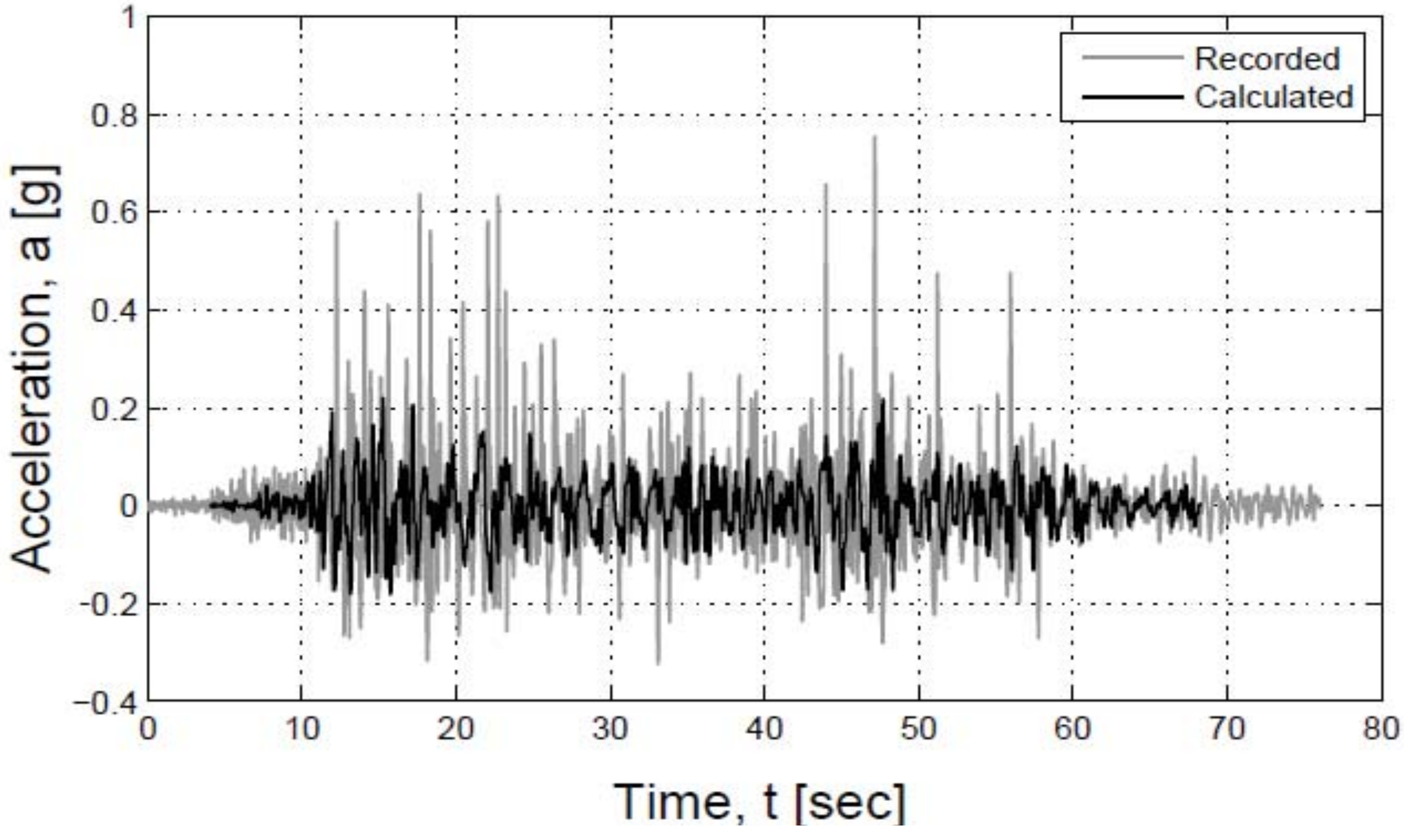

Figure
Click here to download Figure: PelecanosFig09b.eps

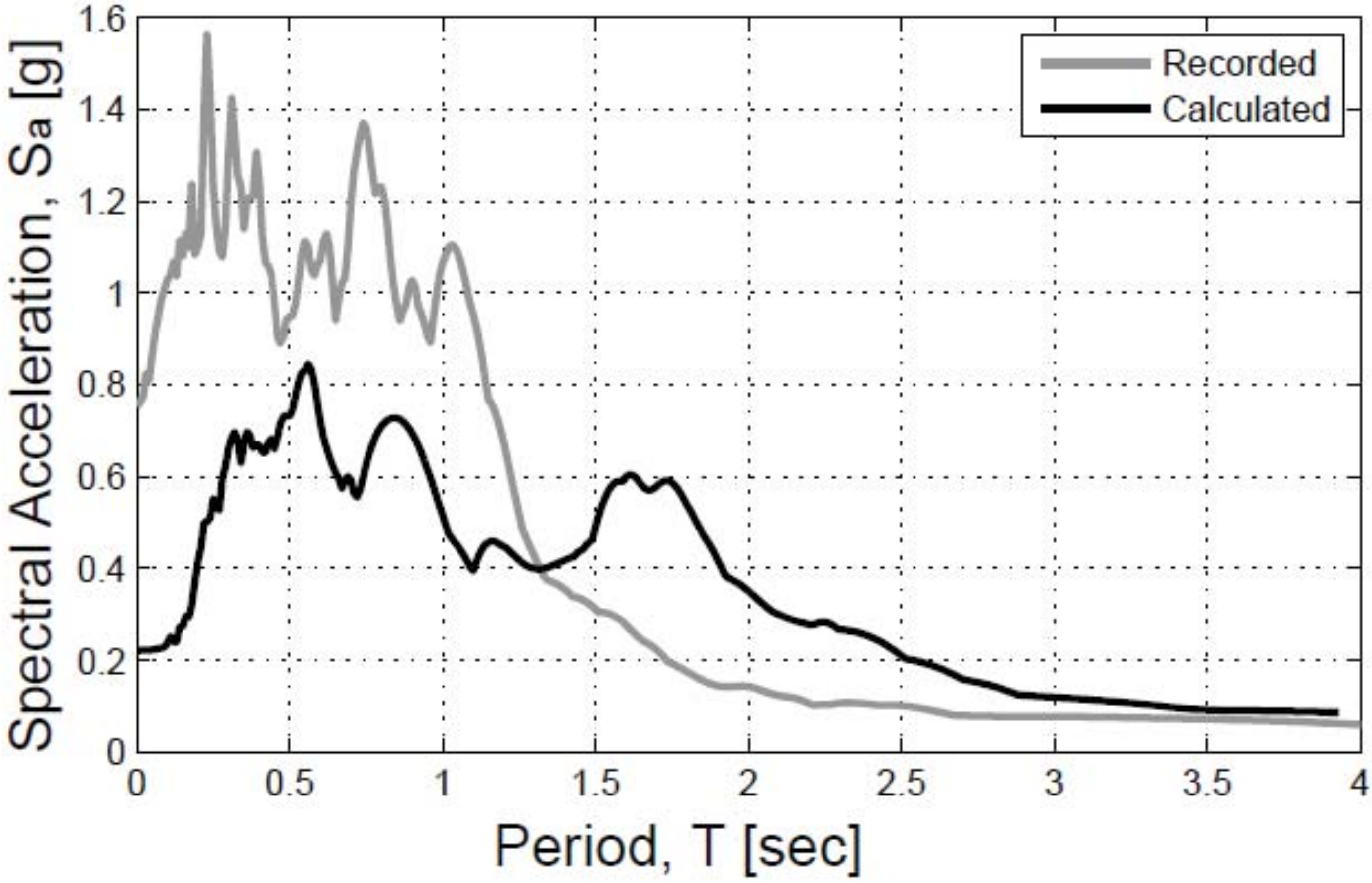

Figure
Click here to download Figure: PelecanosFig10a.eps

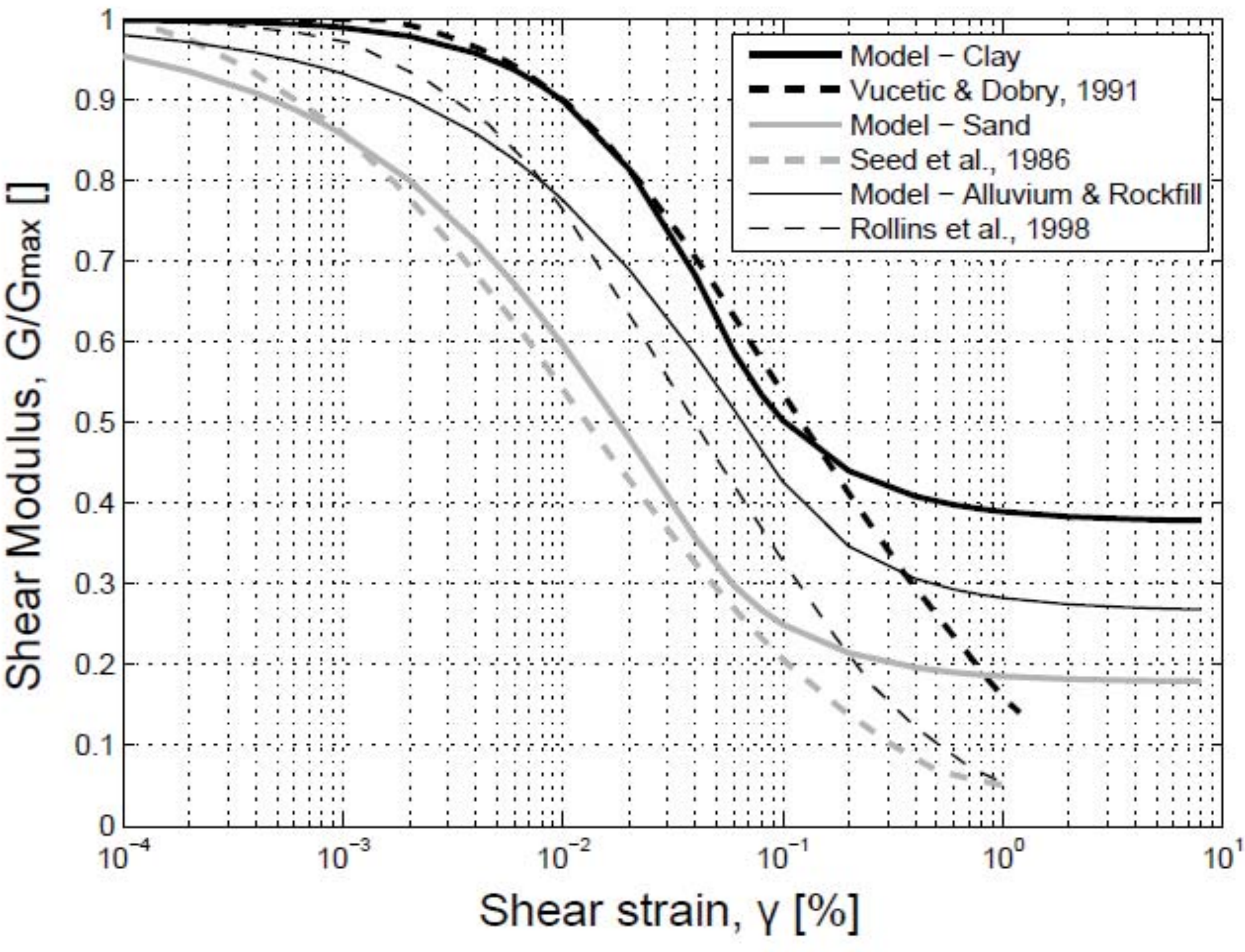

Figure
Click here to download Figure: PelecanosFig10b.eps

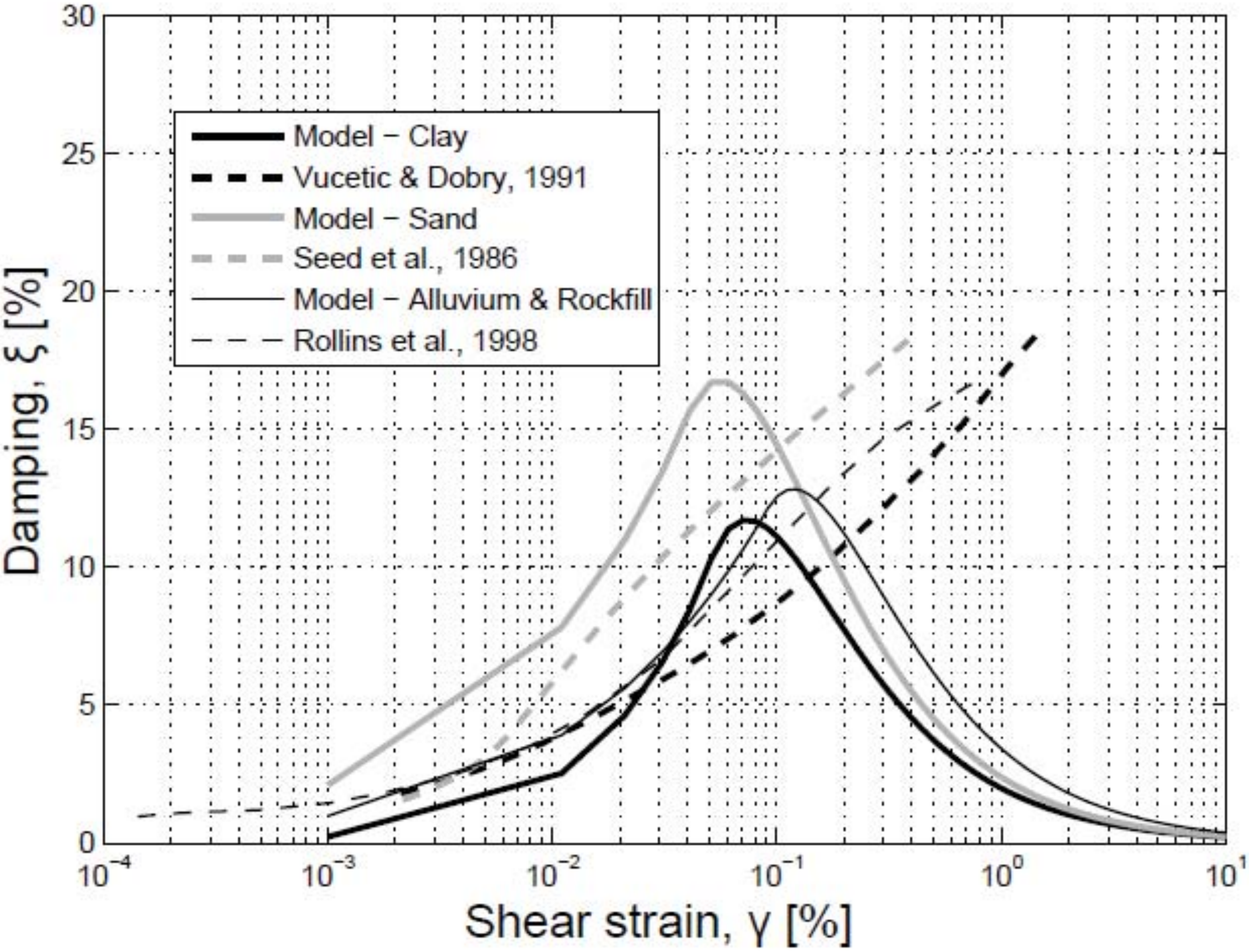

Figure
Click here to download Figure: PelecanosFig11a.eps

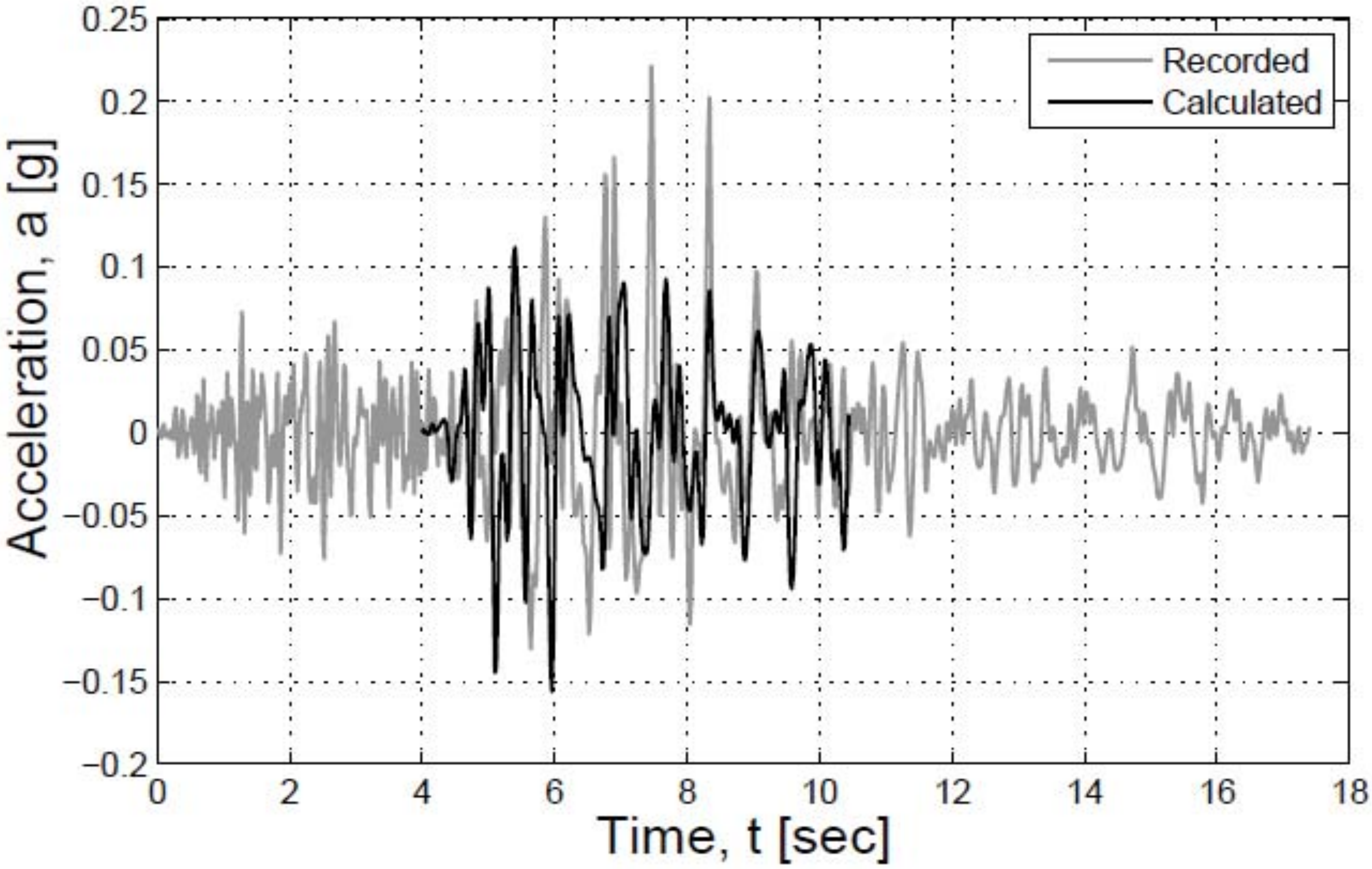

Figure
Click here to download Figure: PelecanosFig11b.eps

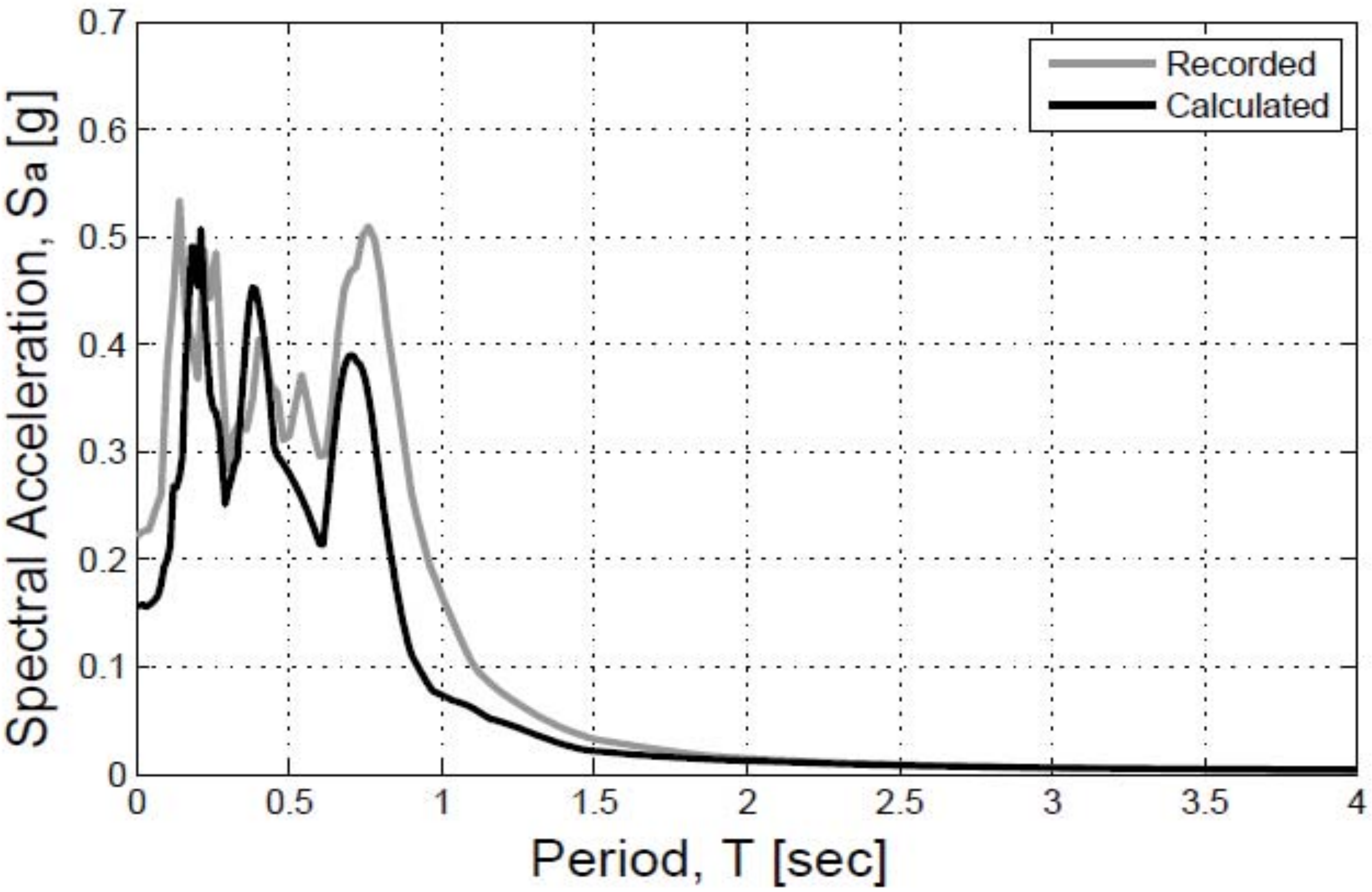

Figure
Click here to download Figure: PelecanosFig12a.eps

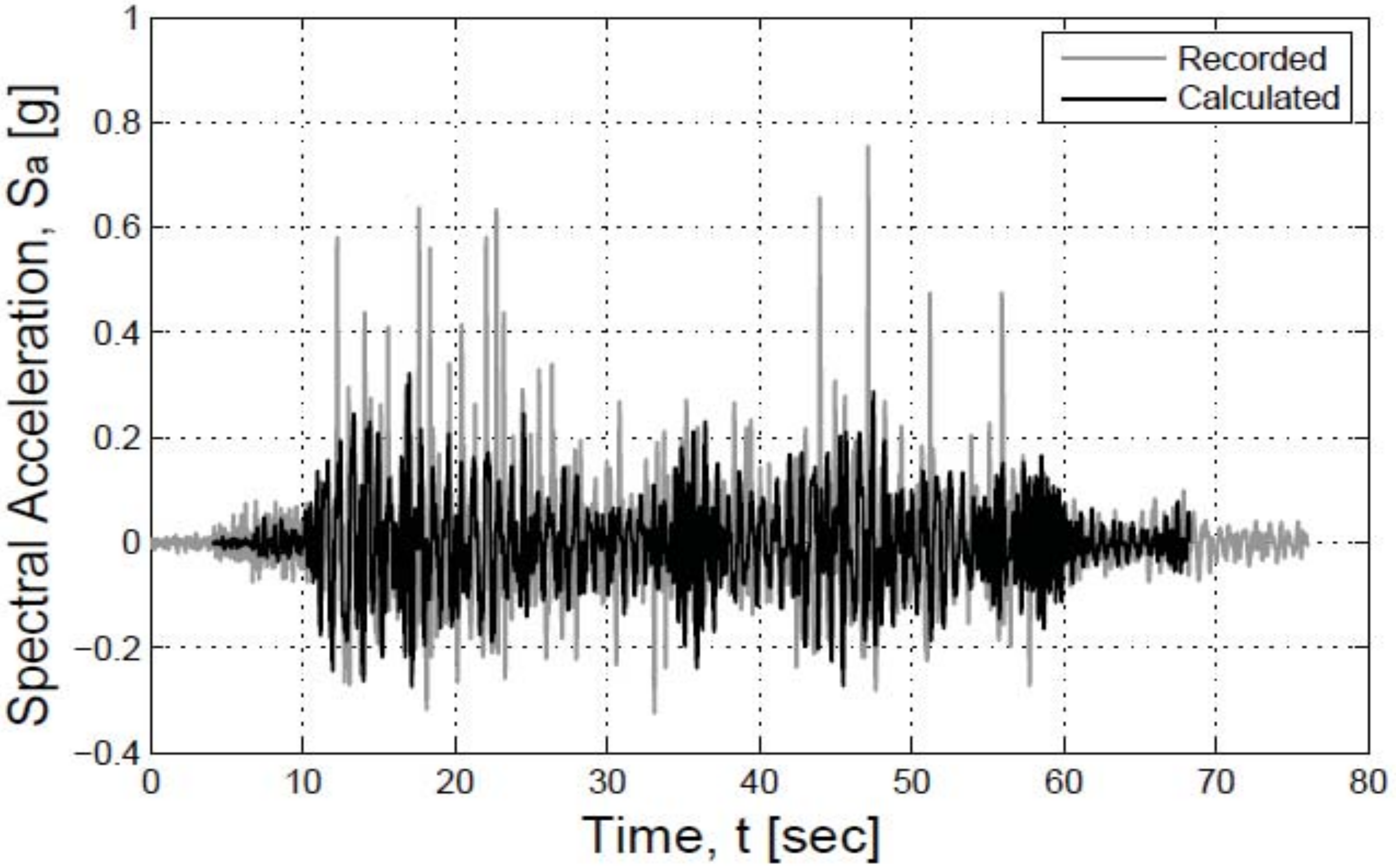

Figure
Click here to download Figure: PelecanosFig12b.eps

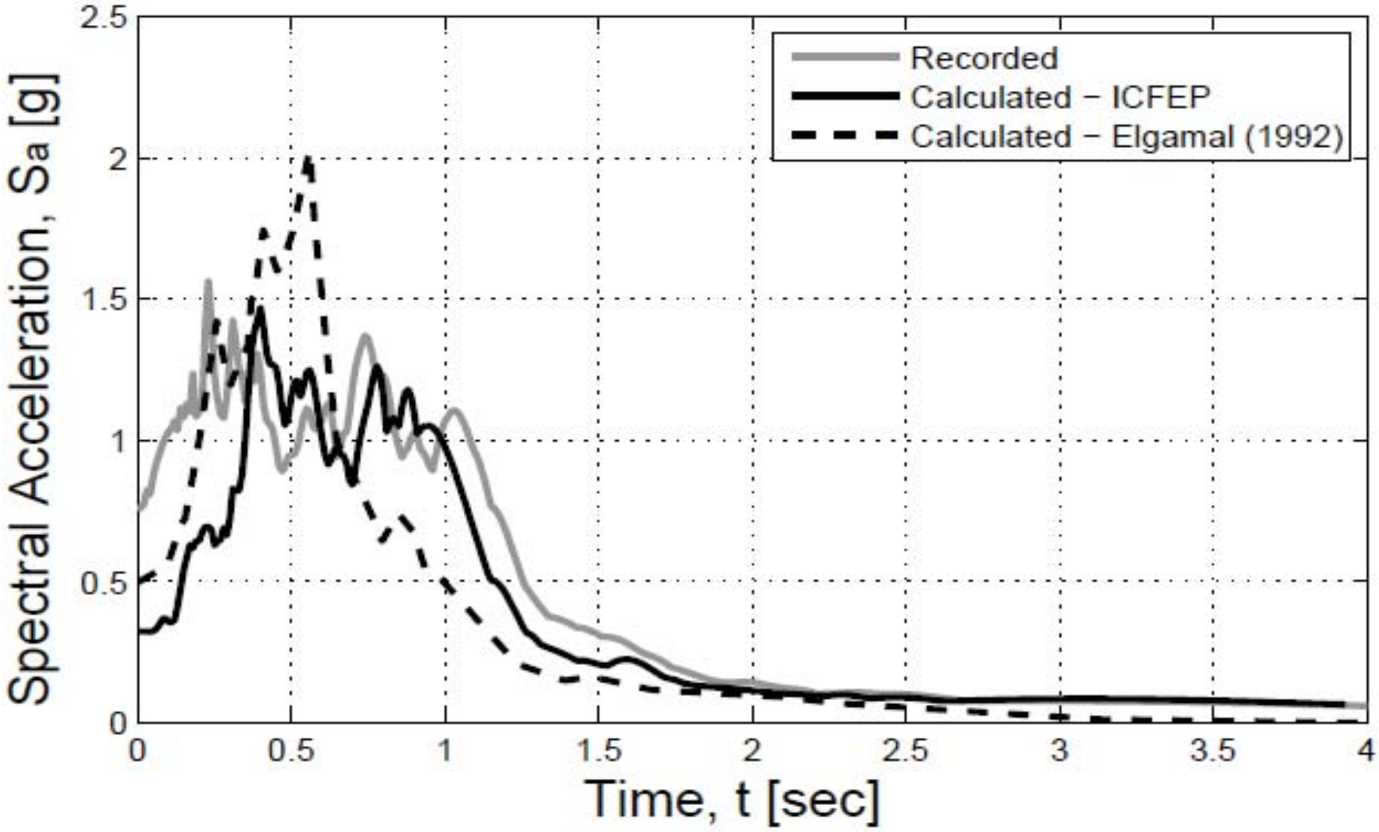

Figure
Click here to download Figure: PelecanosFig13a.eps

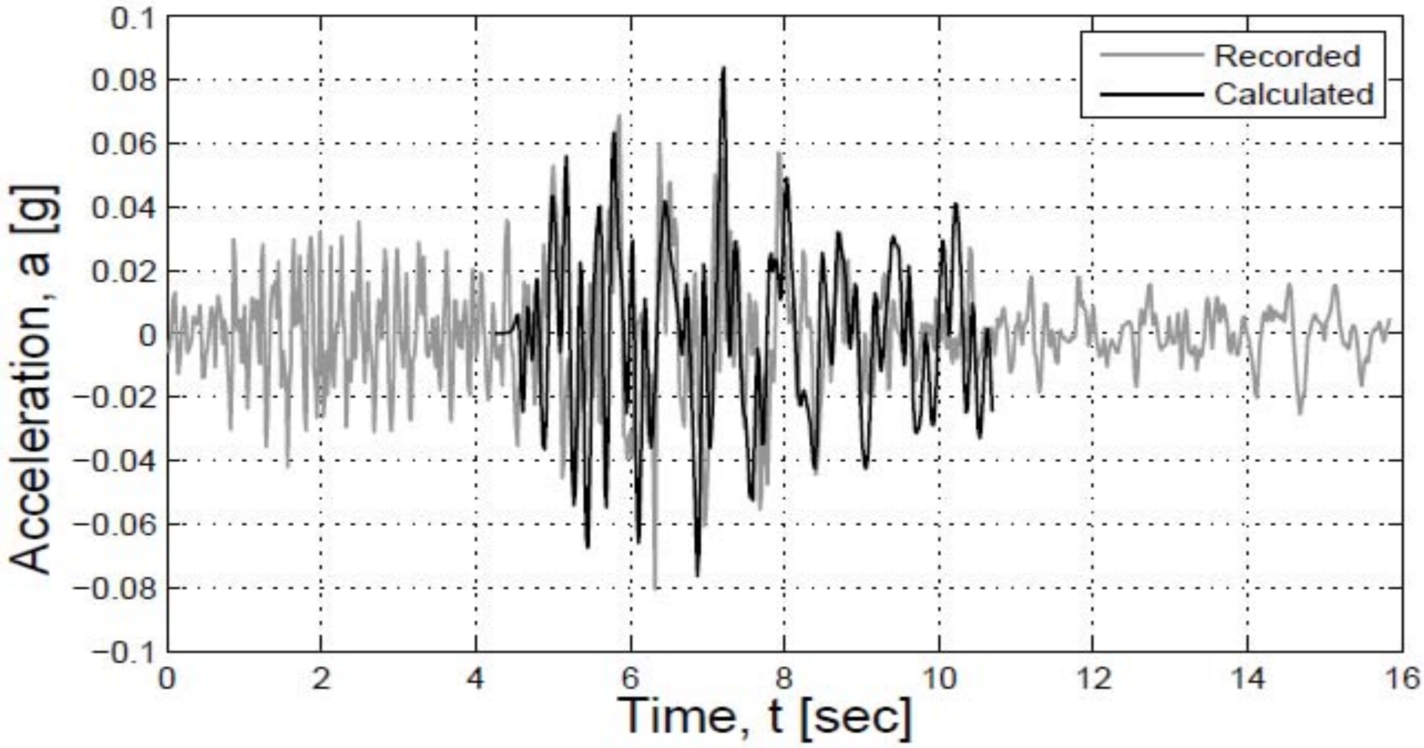

Figure
Click here to download Figure: PelecanosFig13b.eps

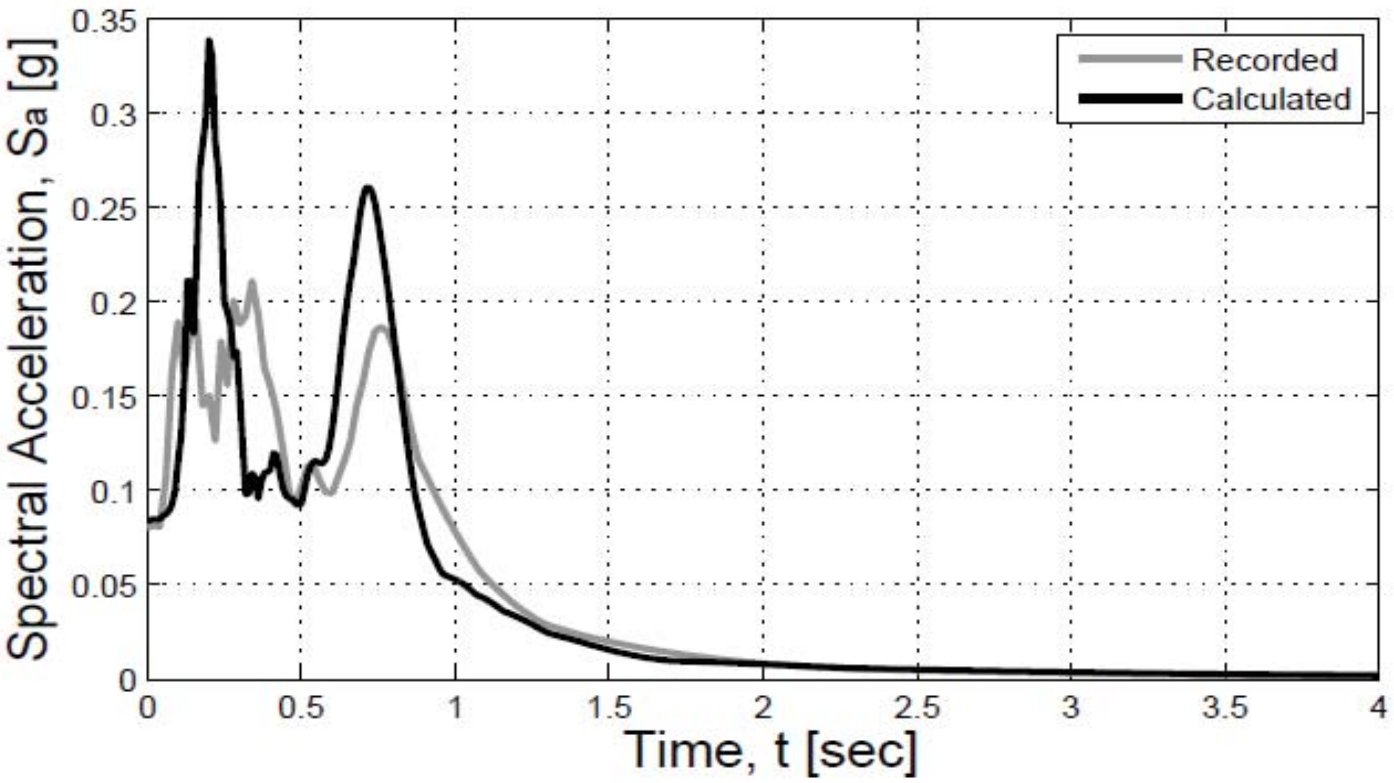

Figure
Click here to download Figure: PelecanosFig14a.eps

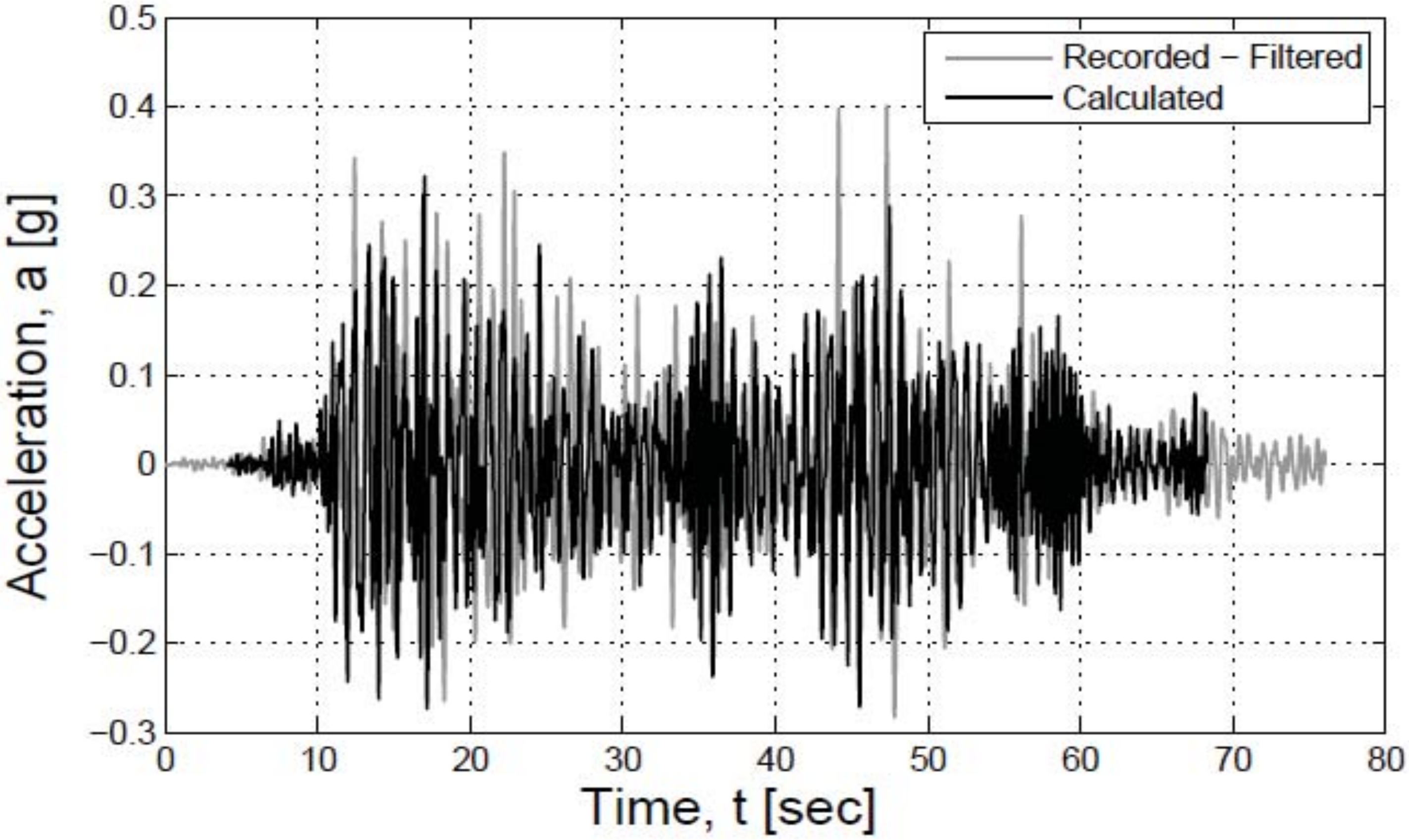

Figure
Click here to download Figure: PelecanosFig14b.eps

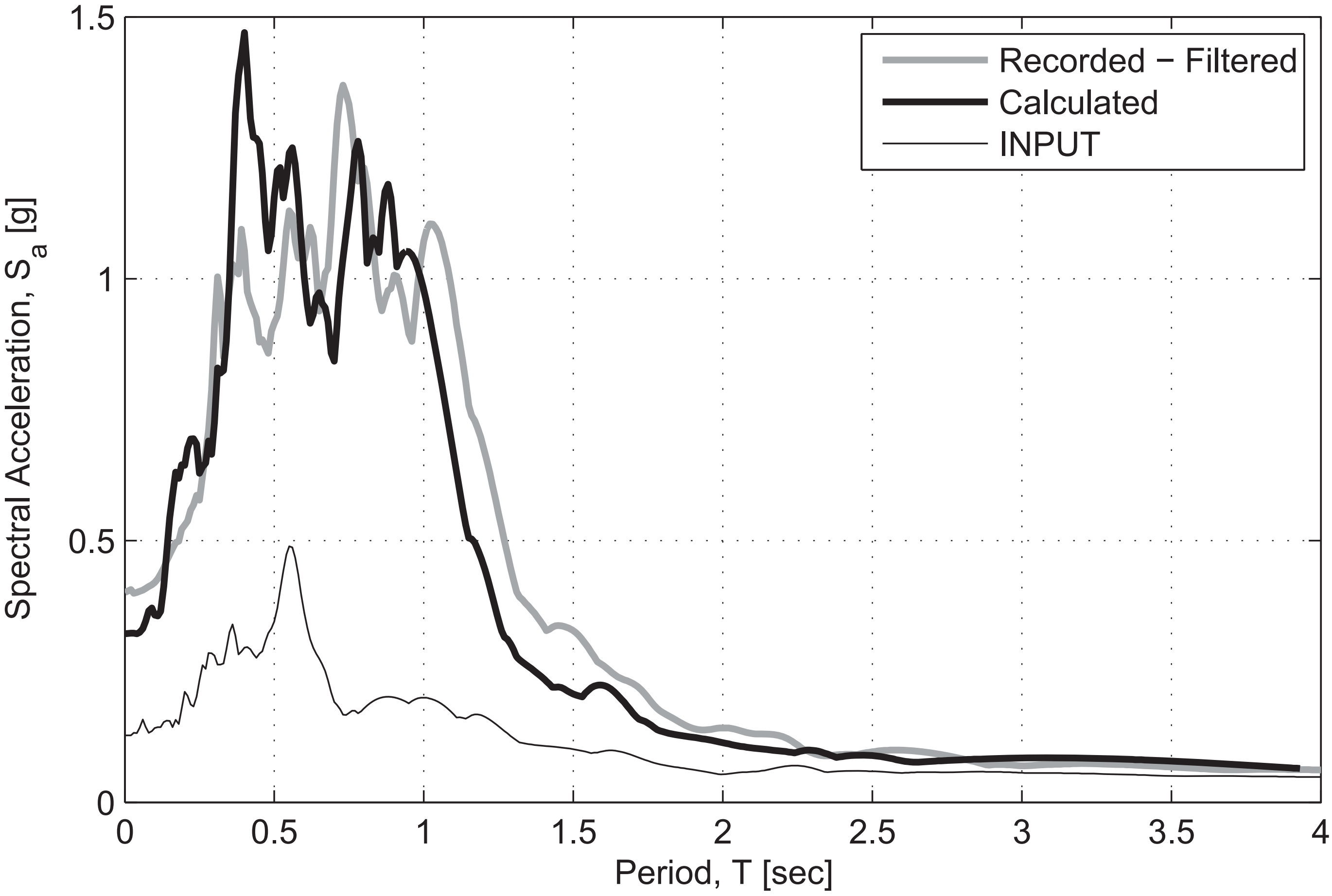

Figure
Click here to download Figure: PelecanosFig15.eps

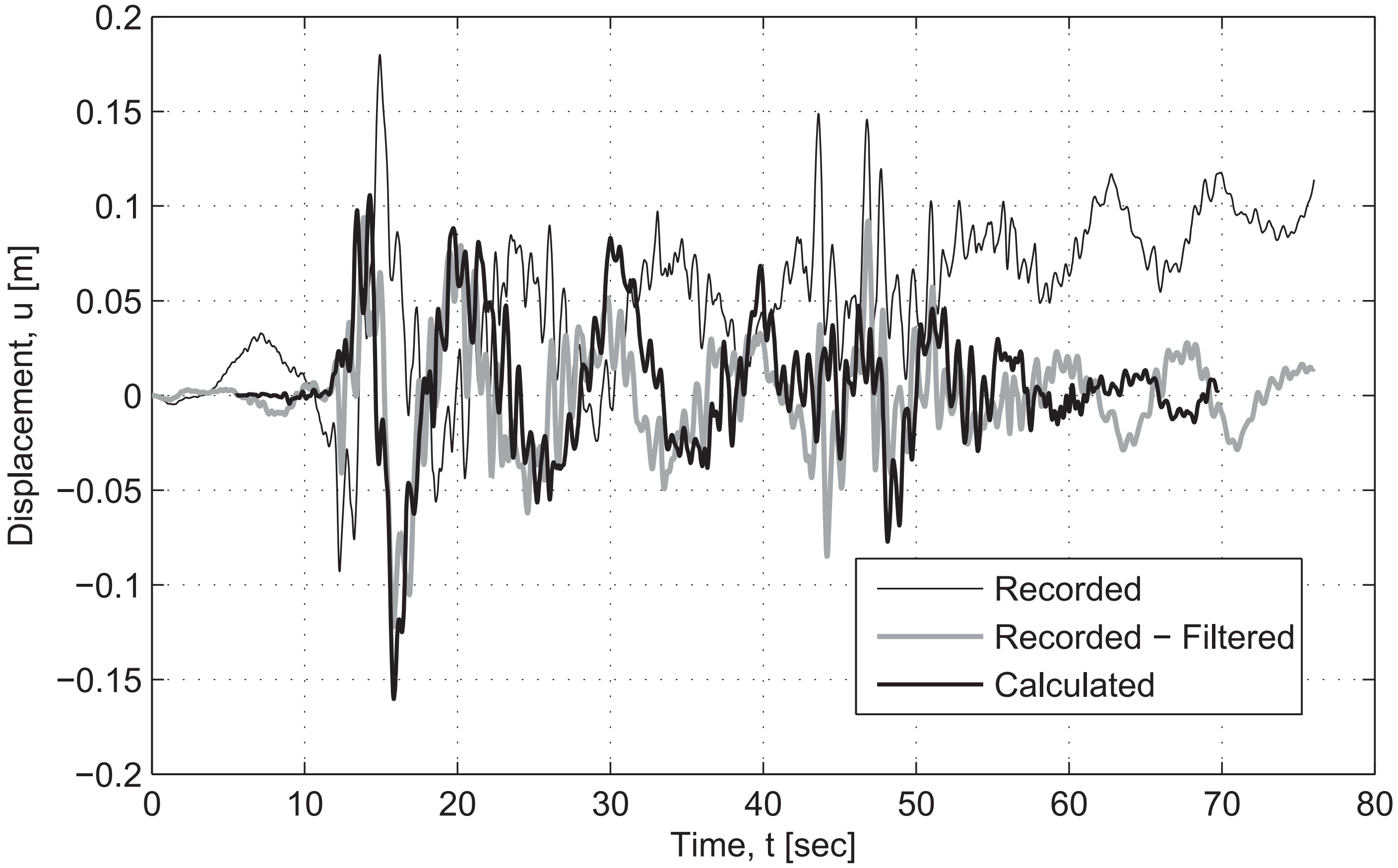

Figure
Click here to download Figure: PelecanosFig16.eps

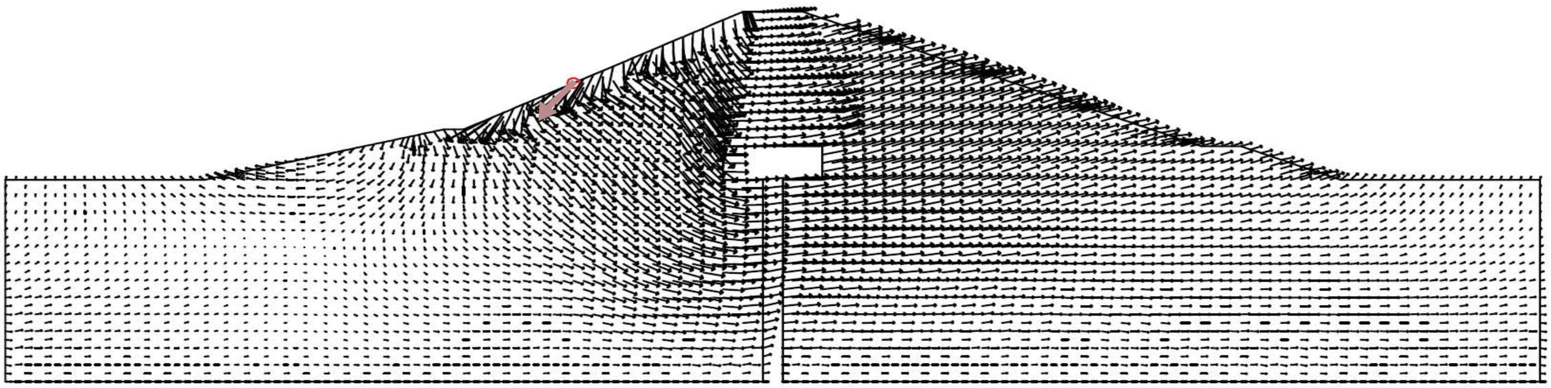

Figure
Click here to download Figure: PelecanosFig17.eps

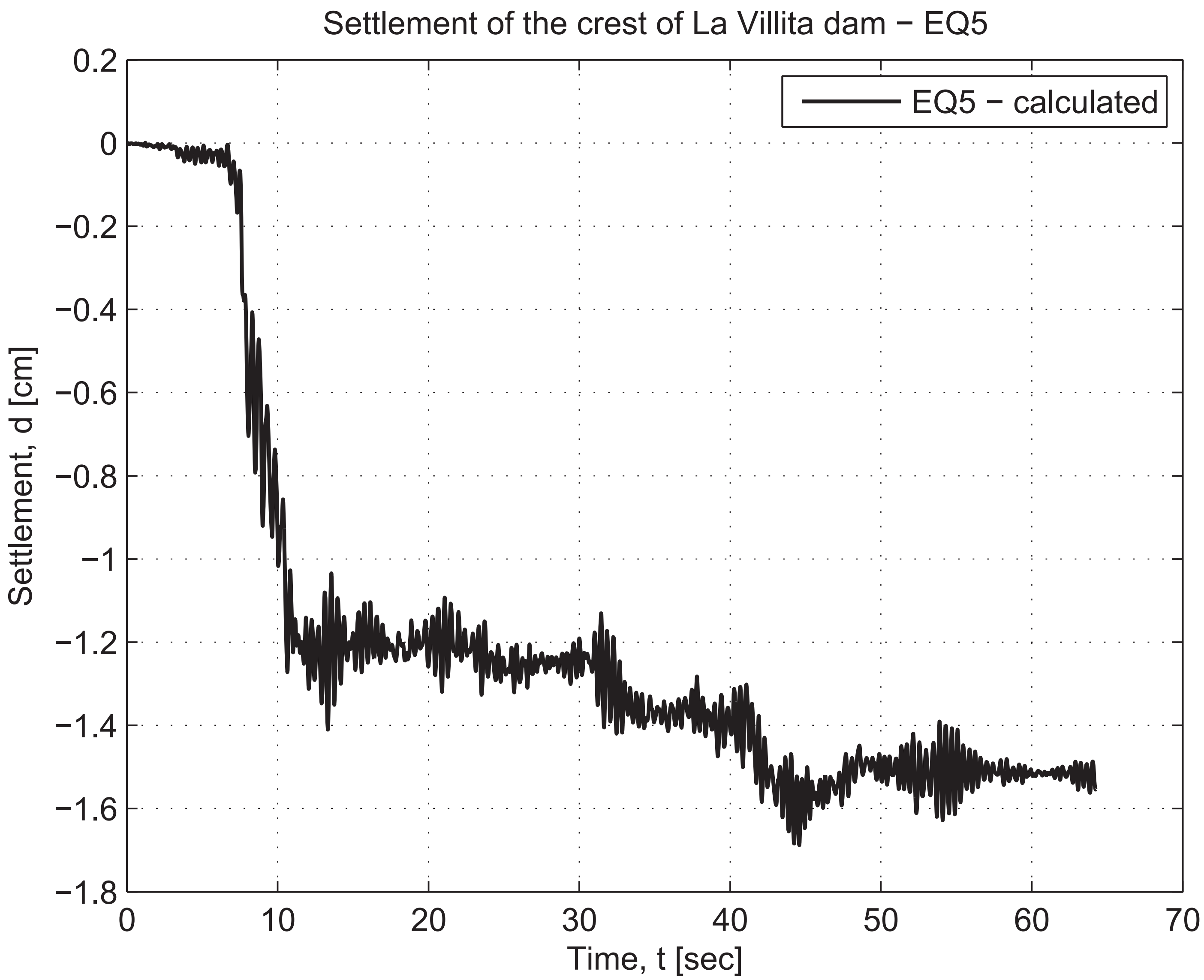

Figure
Click here to download Figure: PelecanosFig18.eps

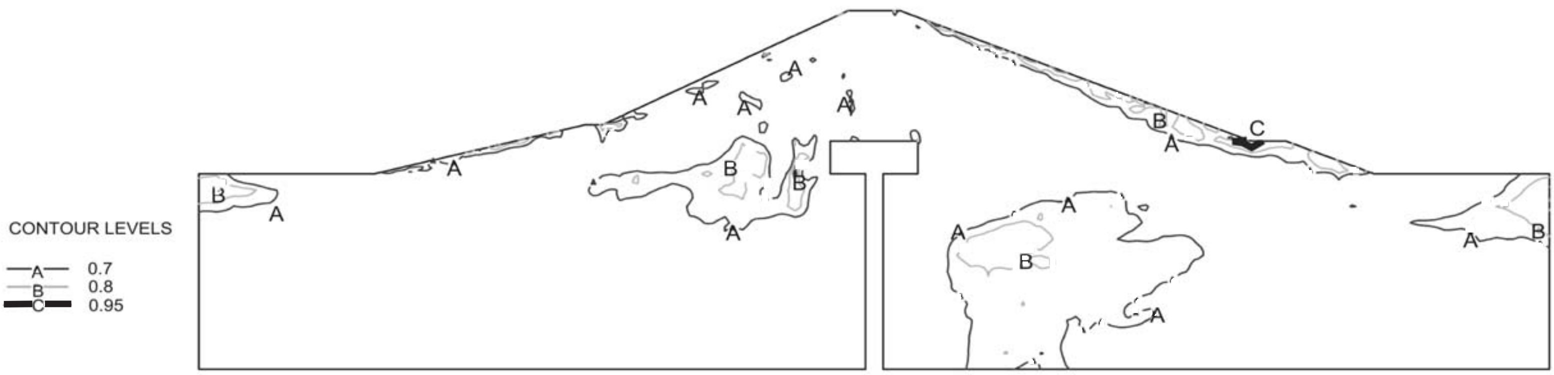

Figure
Click here to download Figure: PelecanosFig19a.eps

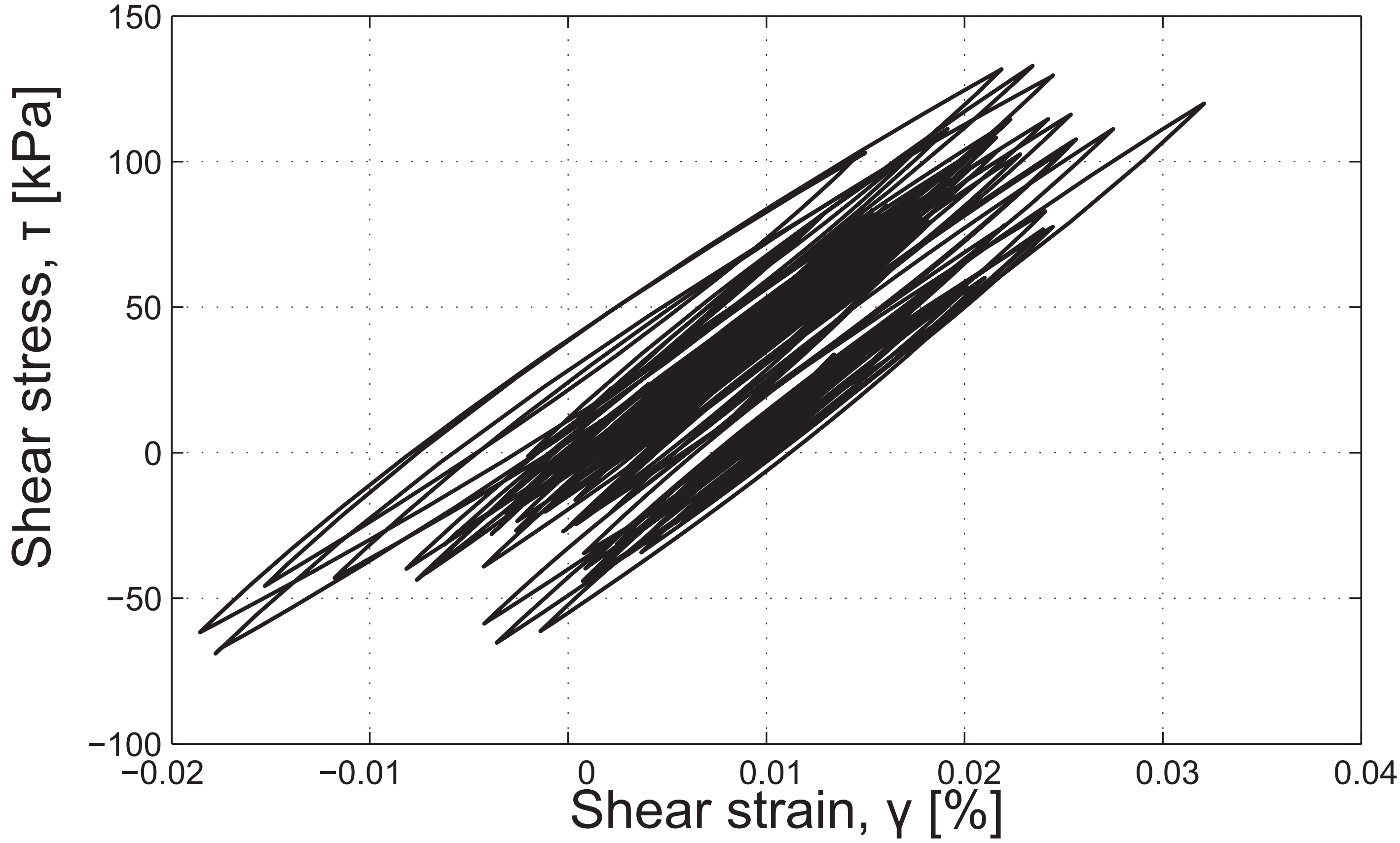

Figure
Click here to download Figure: PelecanosFig19b.eps

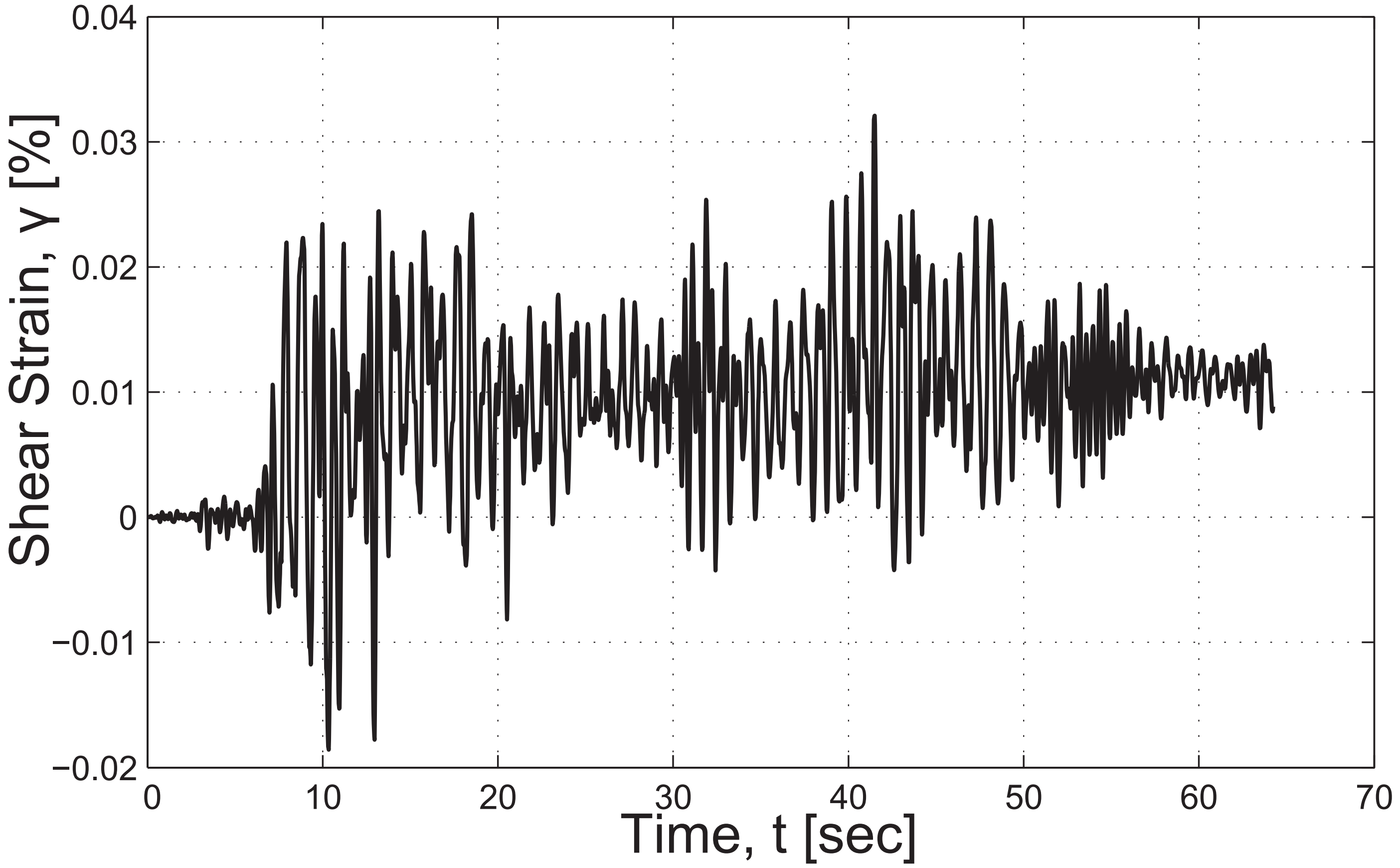

Figure
Click here to download Figure: PelecanosFig20a.eps

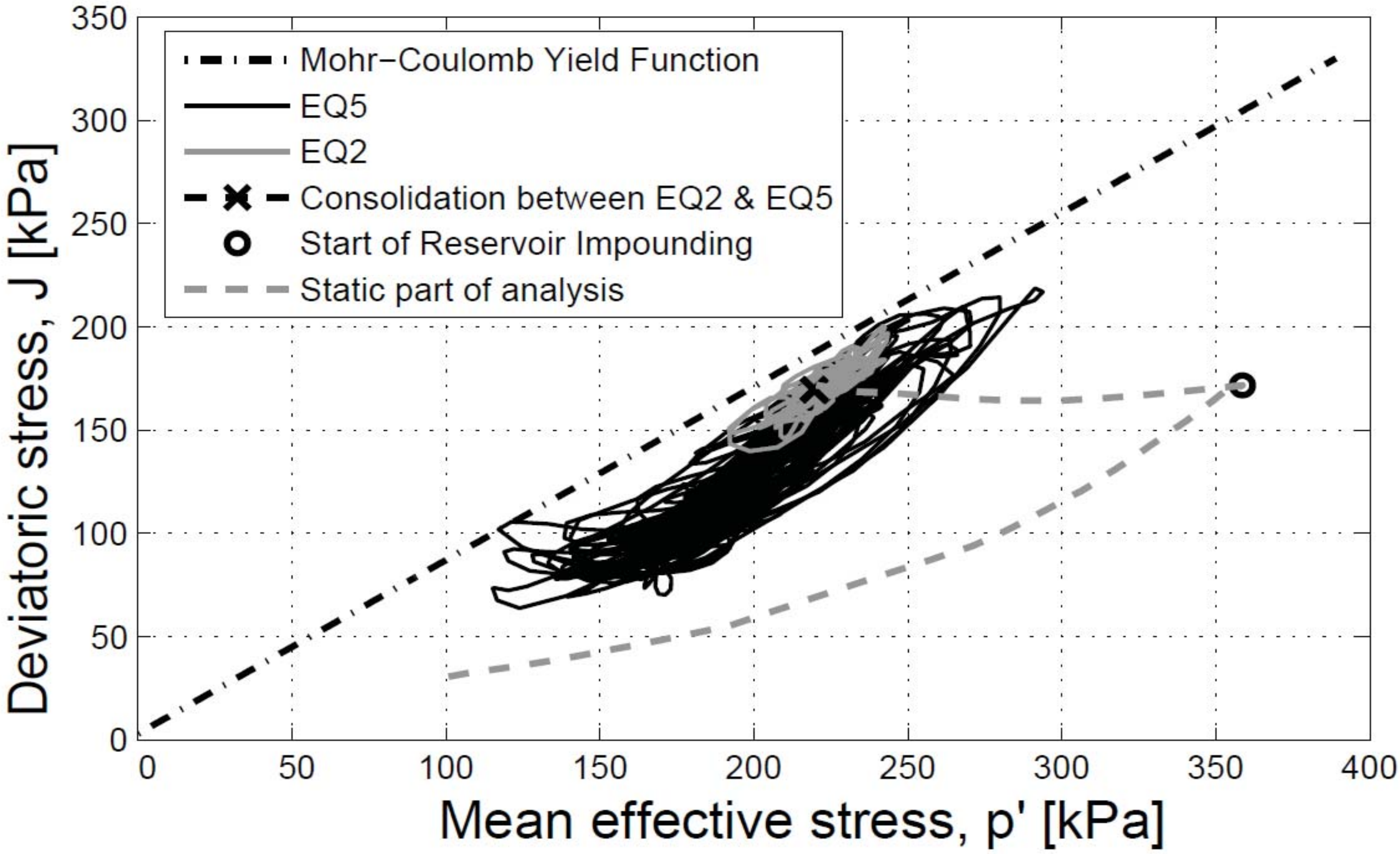

Figure
Click here to download Figure: PelecanosFig20b.eps